



Propargyl amines by aldehyde-amine-acetylene coupling mediated by Ag(I) and Cu(I) complexes of super bulky N-heterocyclic carbenes: Unveiling the role of the super bulky ligands in the coupling reaction

Rajesh Manne^{a,b,1}, Sunita Sharma^{a,1}, Shreyata Dey^{a,1}, Sagar K. Patil^{a,c}, Nidhi Nehra^a, Hemant Rawool^a, Gopalan Rajaraman^{a,*}, Prasenjit Ghosh^{a,*}

^a Department of Chemistry, Indian Institute of Technology Bombay, Powai, Mumbai 400 076, India

^b Symbol Discovery Pvt. Ltd., Plot no 81\1, Road no 13, Phase 1, IDA Mallapur, Hyderabad, Telangana, 500076, India

^c Mettler-Toledo India Private Limited, Amar Hill, Saki Vihar Road, Mumbai 400 072, India

ARTICLE INFO

Keywords:

Silver
Copper
Aldehyde–Amine–Acetylene (A³) coupling
Super bulky N-heterocyclic carbenes (NHCs)
Propargylamines
Homogenous catalysis
DFT studies
Pargyline

ABSTRACT

The copper (1–2)**a** and the silver (1–2)**b** complexes of the super bulky N-heterocyclic carbene (NHC) variants namely, [1,3-{2,4,6-(Ph₂CH)₃C₆H₂}-imidazol-2-ylidene]MX [where, M = Cu; X = Cl (**1a**), Br (**2a**); M = Ag; X = Cl (**1b**), Br (**2b**)] effectively facilitated the A³ coupling reaction of diverse amine, aldehyde, and acetylene substrates yielding a wide array of propargylamines in moderate to good (ca. 24–89 %) yields. A metal bound acetylide species, [1,3-{2,4,6-(Ph₂CH)₃C₆H₂}-imidazol-2-ylidene]M(C≡CPh) [where, M = Cu (A), Ag (B)] has been identified as a key catalytic species by mass spectrometric studies. The Density functional theory (DFT) studies further revealed the rate-limiting step as the formation of the C-C coupling transition state (TS2) from the silver-acetylide species (Int2). The super bulky ligand framework plays a pivotal role in this step by anchoring the protonated Schiff's base imine in the vicinity of the alkyne through several non-covalent-interactions, including a strong C–H...O interaction, thereby reducing the corresponding kinetic barrier leading to an efficient catalytic transformation as reflected in the high propargylamine yields. Furthermore, the catalytic utility of the coupling reaction was further extended by synthesising pargyline, which is a monoamine oxidase B (MAO-B) inhibitor drug molecule, in a one-pot manner and that to in a gram-scale synthesis.

1. Introduction

Many important nitrogen-containing biologically active pharmaceutical and natural products like, Selegiline[1–3] and Rasagiline [4], used in the treatment of early symptoms of Parkinson's disease, and Ladostigil [5,6], a neuroprotective agent, contain propargyl amine core [7]. Hence, the interest in convenient access to propargyl amine scaffolds has seen a surge recently [8,9]. In this regard, the multi-component reaction of the type, Aldehyde–Amine–Acetylene (A³) coupling, has gained prominence, particularly for their step-efficient green approach involving the generation of environmentally benign water as the only by product of the reaction [10–14]. The ease of the A³ coupling is underscored when compared to the traditional routes for the propargyl amine synthesis, which proceed by nucleophilic addition of metal acetylide to an imine, requiring multi-step sequences, with the use of the

stoichiometric amount of air and moisture-sensitive reagents, low temperature and anhydrous conditions [15].

All three substrates, aldehyde, alkyne and amine, of the A³ coupling, being electron-rich and simultaneously unsaturated, require the assistance of a Lewis-acidic transition metal in bringing about the three-component coupling. Consequently, a large number of transition metals in combinations with different ligand types, including that of the catalytically phenomenal N-heterocyclic carbenes, have been explored for the three-component A³ coupling over the past decade [11,12]. However, the influence of super bulky variants of the N-heterocyclic carbenes in A³ coupling remains to be seen. The super bulky N-heterocyclic carbenes, with its deep protective pocket around the catalytically active metal center, provide amenable conditions for substrate activation and subsequent catalysis [16–18]. The challenges associated with the synthesis of super bulky N-heterocyclic carbenes, arising from

* Corresponding author.

E-mail address: pghosh@chem.iitb.ac.in (P. Ghosh).

¹ R. M., S. S. and S. D. contributed equally to this work.

multi-step sequences, severely limit their use in catalysis exploration studies [19–21]. Promising results in a wide array of catalytic transformations have been observed with super bulky N-heterocyclic carbenes. [22–26]

With our interest in the utility of N-heterocyclic carbenes in biomedical applications[27,28] and in chemical catalysis [29–31], we became interested in pursuing Aldehyde–Amine–Acetylene (A^3) coupling [32], in line with our efforts in studying tandem and multi-component reactions [33–39]. We rationalized that because of its deep pockets, the super bulky N-heterocyclic carbenes would provide conducive environment for the catalysis of the three-component reactions.

The coinage metals, *i.e.* silver [40], copper [41], and gold[42] have consistently attracted significant attention due to their exceptional capability to activate carbon-carbon unsaturated bonds. This unique ability enhances the reactivity of alkynes, effectively enabling them to function as robust nucleophiles in the A^3 coupling type reactions. Furthermore, within the domain of A^3 coupling, the theoretical exploration of transition metal carbene complexes has been reported notably limited, although some studies have been reported (see, for example, [43]). The DFT studies on A^3 coupling mediated by (NHC)gold complexes revealed the impact of counter ions on catalytic behaviour[44] and catalytic enhancement facilitated by an acidic environment [45]. Additionally, the investigations of the silver mediated A^3 coupling showed the effect of imine groups on enhancing catalytic activity [46]. The research on Cu catalysts has highlighted the peripheral stabilization of transition states *via* a π -type interaction [47].

Here in the manuscript, we report copper (1–2)**a** and silver (1–2)**b** complexes of super bulky N-heterocyclic carbenes (Fig. 1) that efficiently catalyse the Aldehyde–Amine–Acetylene (A^3) coupling yielding different propargyl amine derivatives in moderate to good yields. Hence, to elucidate the electronic structure, bonding mechanisms, and reactivity patterns of the super bulky copper (1–2)**a** and silver (1–2)**b** complexes in the context of A^3 coupling, meticulous Density Functional Theory (DFT) analyses have been systematically conducted. The DFT calculations provide valuable insights on (i) the intricate interplays between electronic and steric factors that collaborate to heighten the reactivity of these super bulky copper and silver NHC complexes, (ii) the lowest energy pathway through which the A^3 coupling proceeds, and (iii) the rate-limiting step of this reaction, and how does the super bulky NHC ligand design help in alleviate the energy penalty of the rate-limiting step.

2. Results and discussion

Super bulky imidazole-based N-heterocyclic carbene ligand precursors, namely [1,3-{2,4,6-(Ph₂CH)₃C₆H₂}}₂-imidazolium]X [where, X = Cl (1), Br (2)] were synthesized (Scheme 1) from the reaction of 2,4,6-tribenzhydrylaniline, glyoxal and formaldehyde [17,23]. As expected, the characteristic NCHN resonance (δ) appeared downfield shifted [*ca.*

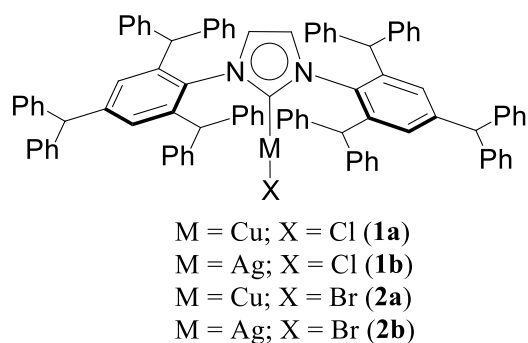


Fig. 1. Copper (1–2)**a** and silver (1–2)**b** complexes of super bulky N-heterocyclic carbenes.

13.00 ppm (1); *ca.*12.39 ppm (2)] in the ¹H NMR spectrum (Supporting Information Figures S27 and S48).

The copper halide (1–2)**a** complexes were synthesized by the reaction of the super bulky imidazolium halide precursors (1) or (2) with Cu₂O in *ca.* 29–37 % yield. The $C_{\text{carbene}}\text{--Cu}$ moiety resonance at 180.5 ppm (2**a**) in the ¹³C{¹H} NMR concurs well with related structurally characterized analogs namely [1,3-{(2,6-Ph₂CH)₂–4-Me-C₆H₂}}imidazol-2-ylidene]CuCl (180.7 ppm) [25], [1,3-{(2,6-Ph₂CH)₂–4–OCH₃-C₆H₂}}imidazol-2-ylidene]CuCl (181.6 ppm) [24], [1,3-{2,4,6-(Ph₂CH)₃C₆H₂}}₂-imidazol-2-ylidene]CuCl (180.4 ppm) [23], [1,3-{(2,6-Ph₂CH)₂–4-Ph₃C₆H₂}}imidazol-2-ylidene]CuCl (180.1 ppm)[23] (Table 1 and Supporting Information Figures S36, S57).

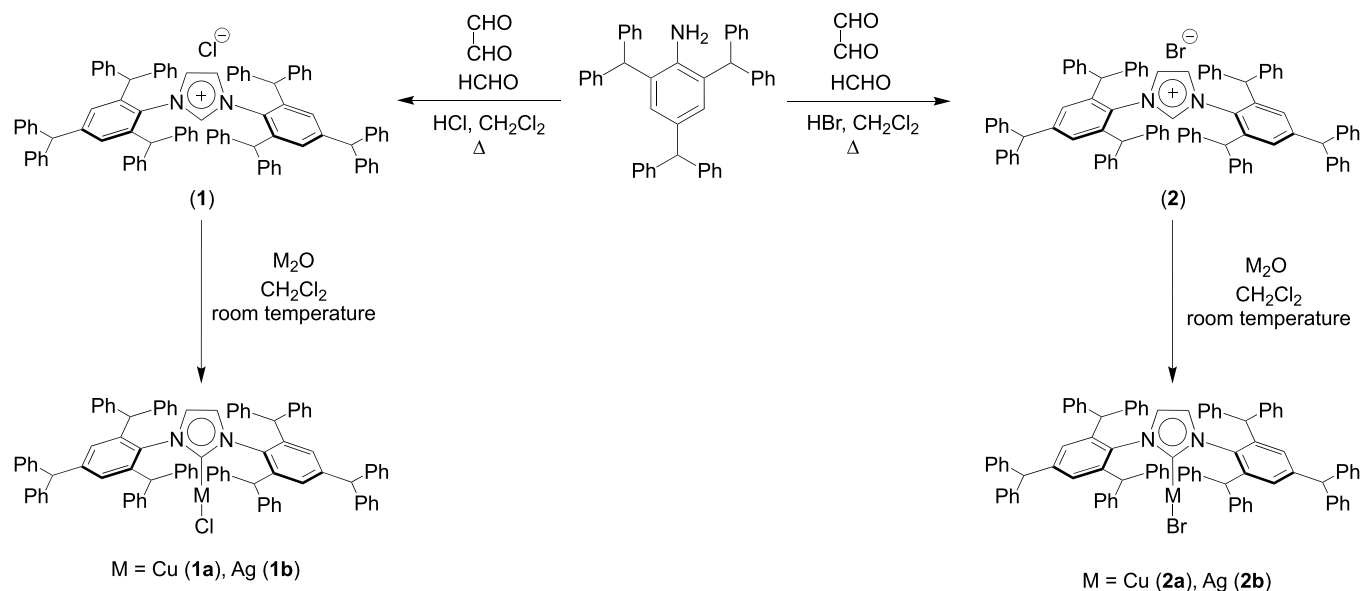
The molecular structure of (2**a**) as determined by single crystal X-ray diffraction technique (Fig. 2), is isostructural with the reported copper chloro (1**a**) analog [23]. The $C_{\text{carbene}}\text{--Cu}$ bond distance of 1.886(5) Å (2**a**) is in good agreement with other structurally characterized examples (Table1), [1,3-{(2,6-Ph₂CH)₂–4-Me-C₆H₂}}imidazol-2-ylidene]CuCl [(1.867(3) Å)[25] [1,3-{(2,6-Ph₂CH)₂–4–OCH₃-C₆H₂}}imidazol-2-ylidene]CuCl [1.875(2) Å] [24], [1,3-{2,4,6-(Ph₂CH)₃C₆H₂}}₂-imidazol-2-ylidene]CuCl [1.885(2) Å] [23], [1,3-{(2,6-Ph₂CH)₂–4-Ph₃C₆H₂}}imidazol-2-ylidene]CuCl [1.8885(18) Å] [23]. The longer Cu–Br bond distance of 2.2129(9) Å in (2**a**) in comparison to the Cu–Cl bond distances of *ca.* 2.0944(9)–2.1004(7) Å in similar structurally characterized examples, is attributed to a larger covalent radius of Br (1.20 Å) to that of Cl (1.02 Å) [48].

The analogous reaction of the imidazolium chloride salt (1) and the imidazolium bromide salt (2) with Ag₂O yielded the silver halide complexes, namely [1,3-{2,4,6-(Ph₂CH)₃C₆H₂}}₂-imidazol-2-ylidene]AgX [where, X = Cl (1**b**), Br (2**b**)]. Here too, in the ¹³C{¹H} NMR spectrum, the characteristic $C_{\text{carbene}}\text{--Ag}$ resonances (δ), were observed at *ca.* 184.4 ppm for 1**b** and *ca.* 184.5 ppm for 2**b** along the lines of *ca.* 184.2 ppm for [1,3-{(2,6-Ph₂CH)₂–4-Me-C₆H₂}}imidazol-2-ylidene]AgCl [19] and *ca.* 185.8 ppm for [1,3-{(2,6-Ph₂CH)₂–4–OCH₃-C₆H₂}}imidazol-2-ylidene]AgCl[24] (Table 2 and Supporting Information Figures S43–S44, S64–S65).

The silver chloro (1**b**) and bromo (2**b**) derivatives are isostructural with the copper bromo (2**a**) complex as observed by the single crystal X-ray diffraction studies. The $C_{\text{carbene}}\text{--Ag}$ bond distances of 2.067(2) Å (1**b**) (Fig. 3) and 2.079(4) Å (2**b**) (Fig. 4) are longer than the copper analog [1.886(5) Å (2**a**)] due a larger covalent radii of Ag (1.46 Å) as compared with Cu (1.29 Å) [49]. The $C_{\text{carbene}}\text{--Ag}$ bond distances of 2.067(2) Å (1**b**) and 2.079(4) Å (2**b**) compares well with the analogous structurally characterized examples, namely, [1,3-{(2,6-Ph₂CH)₂–4-Me-C₆H₂}}imidazol-2-ylidene]AgCl [2.081(2) Å][19] and [1,3-{(2,6-Ph₂CH)₂–4–OCH₃-C₆H₂}}imidazol-2-ylidene]AgCl [2.0803(3) Å][24] (Table 2). Likewise, the Ag–Cl bond distance in 1**b** [2.3027(7) Å] is slightly shorter than the Ag–Br bond distance in 2**b** [2.3988(5) Å] due to a covalent radii difference between Cl (1.02 Å) and Br (1.20 Å) atoms [48].

2.1. Catalysis studies

Significantly enough, all of the copper (1–2)**a** and the silver (1–2)**b** complexes efficiently performed the tandem A^3 coupling of the diverse secondary amines, aliphatic as well as aromatic aldehydes, and acetylene substrates, giving access to various propargylamine compounds. In particular amines, aldehyde and acetylene substrates, when taken in *ca.* 1 : 1 : 1 ratio, and upon treatment with 1 mol % of the copper (1–2)**a** and the silver (1–2)**b** complexes in toluene at 100 °C for 16 h yielded the desired propargylamines (3–27) in moderate to good isolated yields, *ca.* 24–89 % (Table 3). The substrate variation study revealed that secondary amines both cyclic (piperidine, morpholine, pyrrolidine) as well as the acyclic ones (dicyclohexyl, diisopropyl, diethyl etc.), phenyl acetylene with different substituents, 3-ethynylthiophene, TMS acetylene, aliphatic aldehyde (cyclohexyl, isobutyral, formyl) as well as benzaldehyde derivatives both with electron donating and electron



Scheme 1. Synthetic pathway for the copper(I) and silver(I) super bulky N-heterocyclic carbene complexes.

Table 1

Comparison of the metrical data showing C_{carbene}-Cu and Cu-X (X = Cl, Br) bond distances and ¹³C{¹H} NMR chemical shift values for **2a** with the representative examples known in the literature.

Entry	Complex	d(C _{carbene} -Cu) (Å)	d(Cu-X) (X = Cl, Br) (Å)	¹³ C{ ¹ H} NMR (C _{carbene} -Cu) (δ, ppm)	Ref.
1.		1.867(3)	2.0944(9)	180.7	[25]
2.		1.875(2)	2.1044(7)	181.6	[24]
3.		1.885(2)	2.1062(6)	180.4	[23]
4.		1.8885(18)	2.1004(7)	180.1	[23]
5.		1.886(5)	2.2129(9)	180.5	present work

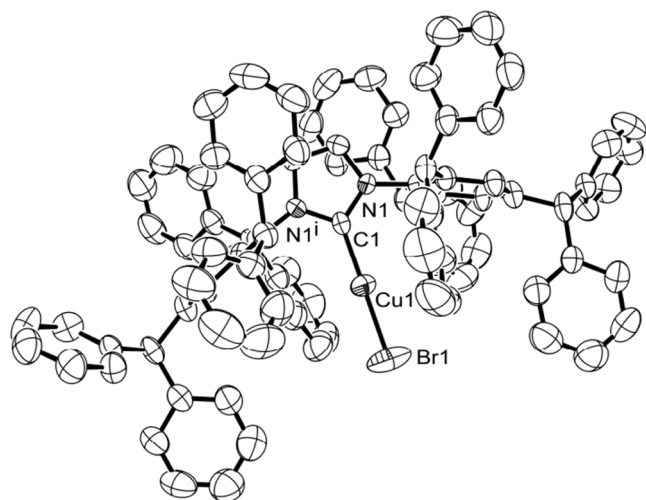


Fig. 2. ORTEP drawing of **2a** with thermal ellipsoids drawn at the 50 % probability level. Selected bond length (Å) and bond angle (°): N(1)–C(1) 1.354 (4), Cu(1)–C(1) 1.886(5), Cu(1)–Br(1) 2.2129(9), N(1)–C(1)–N(1ⁱ) 104.6(4), C(1)–Cu(1)–Br(1) 180.0.

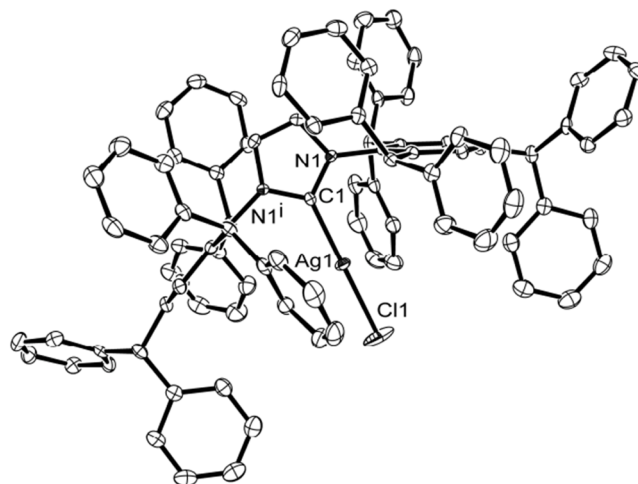
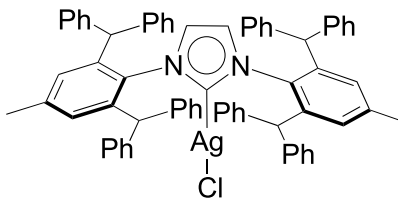
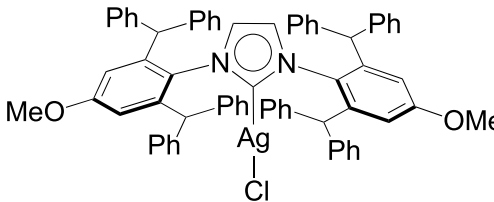
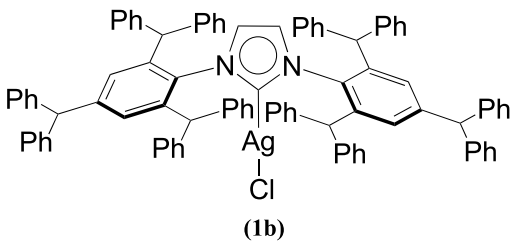
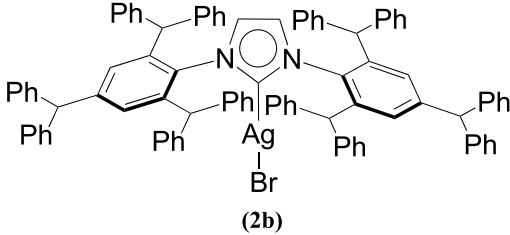


Fig. 3. ORTEP drawing of **1b** with thermal ellipsoids drawn at the 50 % probability level. Selected bond length (Å) and bond angle (°): N(1)–C(1) 1.352 (2), Ag(1)–C(1) 2.067(2), Ag(1)–Cl(1) 2.3027(7), N(1)–C(1)–N(1ⁱ) 104.46 (19), C(1)–Ag(1)–Cl(1) 180.0.

Table 2

Comparison of the metrical data showing $d_{\text{Carbene-Ag}}$ and $d_{\text{Ag-X}}$ ($X = \text{Cl, Br}$) bond distances and $^{13}\text{C}\{^1\text{H}\}$ NMR chemical shift values for **(1–2)b** with the representative examples known in the literature.

Entry	Complex	$d_{\text{Carbene-Ag}}$ (Å)	$d_{\text{Ag-X}}$ ($X = \text{Cl, Br}$) (Å)	$^{13}\text{C}\{^1\text{H}\}$ NMR (Carbene-Ag) (δ , ppm)	Ref.
1.		2.081 (2)	2.3189 (9)	184.2	[19]
2.		2.080(3)	2.3312(8)	185.8	[24]
3.	 (1b)	2.067(2)	2.3027(7)	184.4	present work
4.	 (2b)	2.079(4)	2.3988(5)	184.5	present work

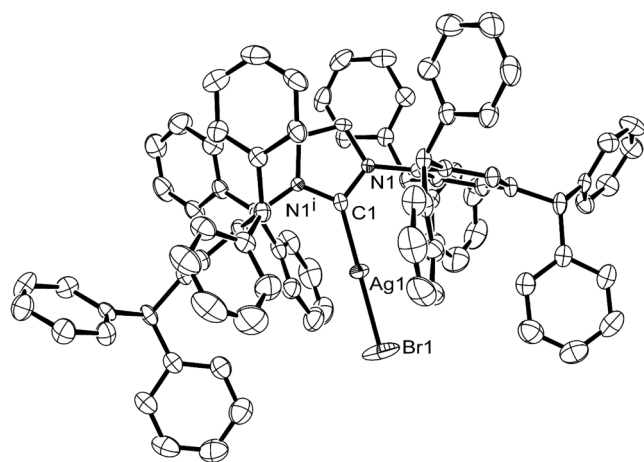


Fig. 4. ORTEP drawing of **2b** with thermal ellipsoids drawn at the 50 % probability level. Selected bond length (Å) and bond angle (°): N(1)–C(1) 1.346 (3), Ag(1)–C(1) 2.079(4), Ag(1)–Br(1) 2.3988(5), N(1)–C(1)–N(1¹) 104.9(3), C(1)–Ag(1)–Br(1) 180.0.

withdrawing groups yielded the corresponding propargylamines in appreciable yield as showed in [Table 3](#).

The control and blank run experiments confirmed the active participation of copper (**1–2a**) and the silver (**1–2b**) complexes in catalysis as observed from the significant enhancement of the isolated product yields of ca. 80 % (**1a**), ca. 73 % (**1b**), ca. 88 % (**2a**) and ca. 79 % (**2b**) when compared to that with the respective metal precursors, namely, CuCl (20 %), AgCl (15 %), CuBr (9 %) and AgBr (21 %) for the A^3 coupling of the representative phenyl acetylene, isobutyraldehyde and morpholine substrates (Supporting Information Tables S2 and S3). Interestingly, the copper chloro (**1a**) and the bromo (**2a**) derivatives performed better than their silver (**1b**) and (**2b**) counterparts, respectively.

Only a handful of reports exist on the use of well-defined molecular complexes of coinage metals and the N-heterocyclic carbene ligands in the A^3 coupling [[45,50–55](#)], and copper remain the least explored among its group [[56,57](#)]. Despite these reports [[45,50–56,58](#)], we synthesized representative benchmark complexes, namely [1,3-(2,4,6-Me₃C₆H₂)₂-imidazol-2-ylidene]CuCl [[59,60](#)], [1,3-(2,4,6-Me₃C₆H₂)₂-imidazol-2-ylidene]AgCl [[60](#)], [1,3-(2,6-*i*-Pr₂C₆H₃)₂-imidazol-2-ylidene]CuBr [[61](#)], [1,3-(2,6-*i*-Pr₂C₆H₃)₂-imidazol-2-ylidene]AgBr [[62](#)] and [2,6-*bis*-(1-(1*S*)-menthyl-3-methylene-imidazol-2-ylidene)-pyridine]Ag₂Cl₂ [[32](#)], for obtaining a direct comparison of the catalytic activity with that of the copper (**1–2a**) and silver (**1–2b**) complexes. Specifically, for the following phenylacetylene, isobutyraldehyde, and morpholine substrates, significant enhancements of the catalysis yield of the product, 4-(3-phenylprop-2-yn-1-yl)morpholine (**5**), to the amount of ca. 73–80 % for the copper (**1–2a**) complexes were observed as opposed to that of ca. 36–40 % obtained with the benchmark [1,3-(2,4,6-Me₃C₆H₂)₂-imidazol-2-ylidene]CuCl [[59,60](#)] and [1,3-(2,6-*i*-Pr₂C₆H₃)₂-imidazol-2-ylidene]CuBr [[61](#)] complexes (Entries 1 and 3 Supporting Information Table S4). Similar enhancement of the product (**5**) yield of ca. 79–88 % were seen for the silver (**1–2b**) complexes against the corresponding yields of ca. 24–34 % in case of the benchmark [1,3-(2,4,9-Me₃C₆H₂)₂-imidazol-2-ylidene]AgCl [[60](#)] and [1,3-(2,6-*i*-Pr₂C₆H₃)₂-imidazol-2-ylidene]AgBr complexes [[62](#)] (Entries 2 and 4 Supporting Information Table S4). The sterically demanding copper (**1–2a**) and silver (**1–2b**) complexes exhibited superior catalytic activities thus favouring the influence of the super bulky N-heterocyclic carbene ligands.

The superiority of these copper (**1–2a**) and silver (**1–2b**) complexes of the super bulky N-heterocyclic carbenes can be easily gauged from a comparison of its catalysis performances made in [Table 4](#) with the

relevant well-defined molecular complexes of non-bulky N-heterocyclic carbene ligands that exist in the literature for the A^3 coupling of the following representative substrates, phenyl acetylene, formaldehyde and piperidine producing the product, 1-(3-phenylprop-2-yn-1-yl)piperidine (**23**). For the sake of uniformity, the catalyst loading was calculated with respect to the number of metal centers present in the respective catalyst, owing to the existence of both mononuclear as well as binuclear complexes in the table. The Au(I) complex, namely [1-{CH₂CH(OCH₃)C₆H₅}-3-CH₃-imidazol-2-ylidene]AuCl [[45](#)] exhibited near quantitative conversion of ca. 88 % based on ¹H NMR at 8 hours of reaction time at 80 °C but at higher catalyst loading of 3 mol % in comparison to that of 1 mol % for the super bulky NHC complexes (**1–2a**) and (**1–2b**) showing moderate to good isolated yields of ca. 41–52 % ([Table 4](#)). Again, in dichloromethane at room temperature, the binuclear silver and gold complexes, 2,6-*bis*-(1-(1*S*)-menthyl-3-methylene-imidazol-2-ylidene)-pyridine]M₂Cl₂ [M=Ag, Au] [[32](#)] showed isolated yields of ca. 48–51 % but with a higher catalyst loading of 2 mol %. In light of these studies, the catalysis yields exhibited by the super bulky NHC complexes (**1–2a**) and (**1–2b**) complexes are indeed promising and would usher further research into the area.

In order to test the more meaningful and impactful synthetic utility of our A^3 -coupling protocol, the one-pot coupling reaction was successfully employed to synthesize the drug molecule pargyline [[63](#)], an inhibitor of monoamine oxidase B (MAO-B), as outlined in [Scheme 2](#). To our delight, the reaction between TMS acetylene, N-methyl-1-phenylmethanamine and formaldehyde at 100 °C and 1 mol % catalyst loading (**1a/1b/2a/2b**) for 16 hours, followed by the treatment with base K₂CO₃ at room temperature for 3 hours, yielded the desired product pargyline (**28**) in good yield (45–67 %). Even, Furthermore, the gram-scale synthesis of pargyline was achieved for a representative catalyst (**1a**) in appreciable yield of 1.01 g (63 %) on a 10 mmol scale reaction. .

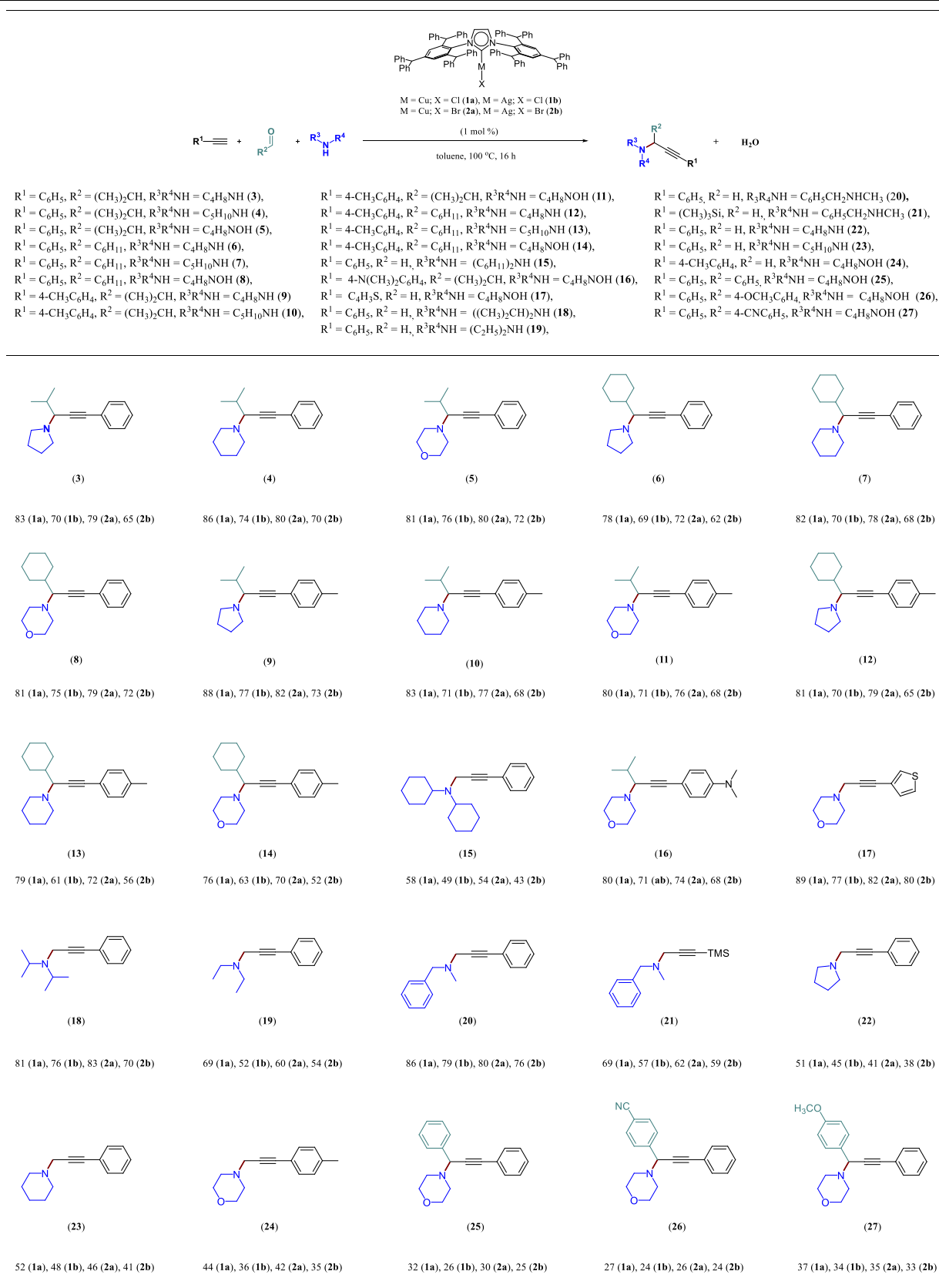
A proposed catalytic cycle, proceeds *via* a common metal bound acetylide species, [1,3-{2,4,6-(Ph₂CH)₃C₆H₂}-2-imidazol-2-ylidene]M (C≡CPh) [where, M = Cu (**A**), Ag (**B**)], which is formed from the copper (**1–2a**) and the silver (**1–2b**) complexes ([Scheme 3](#)). Both of the metal bound acetylide species have been characterized by mass spectrometry as observed from the [M + Na]⁺ peaks at *m/z* 1404.5304 (Calcd. 1404.5308) for the copper bound acetylide (**A**) species ([Fig. 5](#) and Supporting Information Figure S69) and at *m/z* 1449.5059 (Calcd. 1449.5054) for the silver bound acetylide (**B**) species ([Fig. 6](#) and Supporting Information Figure S70). Subsequent reaction of the copper bound acetylide (**A**) species and the silver bound acetylide (**B**) species with the protonated Schiff's base imine gave the desired propargylamine product along with the regeneration of the copper (**1–2a**) and the silver (**1–2b**) complexes.

The X-ray photoelectron spectroscopy (XPS) analysis provided valuable insight about the mechanism of the coupling reaction. In particular, the copper 2p core-level peaks of complex (**2a**) were observed at 931.3 eV (Cu 2p_{3/2}) and 951.1 eV (Cu 2p_{1/2}) [[64](#)], whereas silver 3d core-level peaks of complex (**2b**) were observed at 368.7 eV (Ag 3d_{5/2}) and 374.8 eV (Ag 3d_{3/2}) [[65](#)], and which are consistent with the (+1) oxidation state of both the metal center. Significantly enough, peaks of similar values were observed when the XPS data was inspected of both the complexes after treatment with phenylacetylene, isobutyraldehyde and morpholine for 16 h at 100 °C *i.e.* under the catalysis conditions. This observation further confirmed the involvement of M(I) [M = Cu, Ag] oxidation state in the catalytic cycle ([Figs. 7 and 8](#) and Supporting Information Figures S175–S178).

2.2. Density functional theory studies

DFT calculations were carried out employing the Gaussian 09 software suite [[66–69](#)]. To undertake an in-depth theoretical examination of the electronic structure, bonding, and reactivity involved in this reaction, we employed the B3LYP-D3 functional [[70,71](#)] along with a

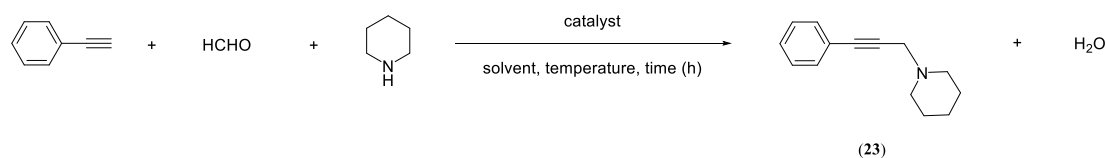
Table 3

Selected results for the copper (1–2)a and the silver (1–2)b complexes catalyzed aldehyde-amine-acetylene (A^3) coupling yielding propargylamines.

(a). Reaction conditions: 1:1:1 ratio of aldehyde:amine:acetylene, 1 mol % of catalyst (1a/1b/2a/2b), 5.0 mL of toluene at 100 °C for 16 hours. Isolated yields are reported.

Table 4

A comparison of A³ coupling reaction of representative piperidine, phenyl acetylene and formaldehyde substrates as catalyzed by well-defined transition metal-NHC complexes known in literature.



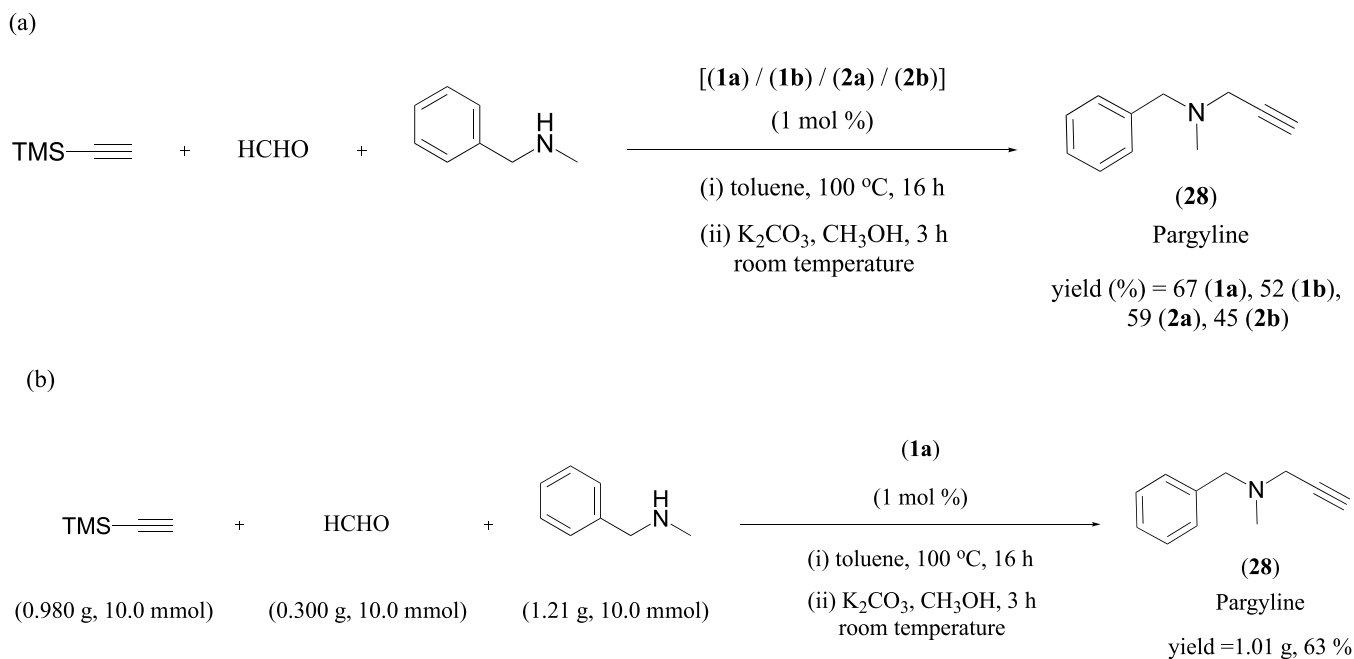
S.No	Catalyst	Time (h)	Solvent	Catalyst loading (mol %)	Temperature (°C)	Yield ^a (%)	Reference
1.		8	H ₂ O	3	80	88 ^b	[45]
2.		24	CH ₂ Cl ₂	2	30	51 ^a	[32]
3.		24	CH ₂ Cl ₂	2	30	48 ^a	[32]
4.		16	toluene	1	100	52 ^a	this work
5.		16	toluene	1	100	48 ^a	this work
6.		16	toluene	1	100	46 ^a	this work
7.		16	toluene	1	100	41 ^a	this work

^a Isolated yield

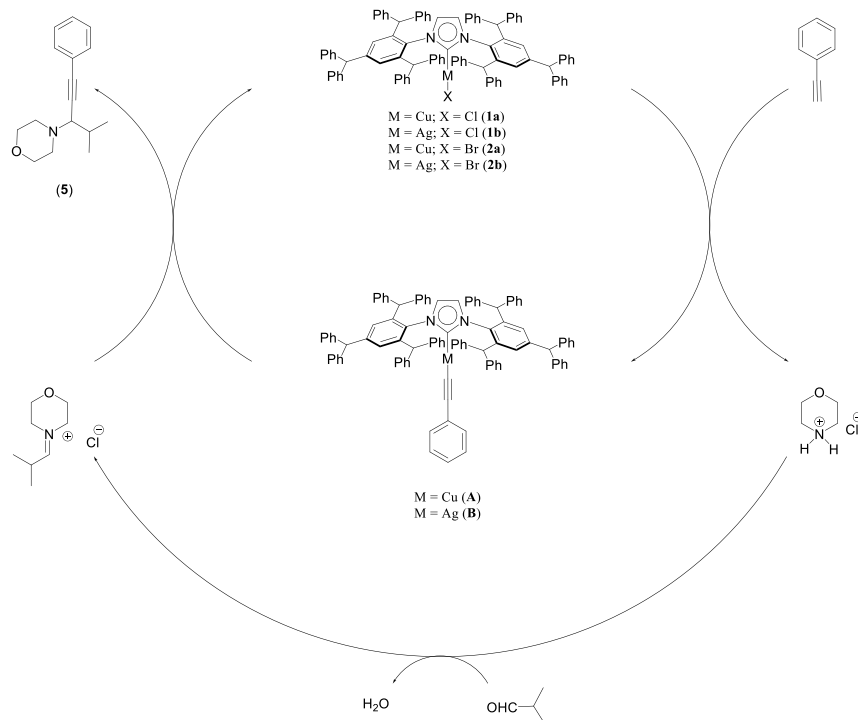
^b ¹H NMR yield.

combination of the SDD basis set [72] for the copper and silver metal center and the 6-31G* basis set for the other atoms [70,71,73,74]. To improve the precision of gas-phase energy evaluations, a single-point calculation was conducted employing elevated basis sets, notably TZVP for the non-metal atoms [75] and SDD for the gold metal center. Furthermore, the Polarizable Continuum Model (PCM) solvation model was integrated into the analysis [76]. To perform a thorough bonding analysis, diverse forms of bonding calculations were executed. The bond

parameters obtained from the optimized geometries of copper (1-2)a and the silver (1-2)b complexes demonstrate strong agreement with X-ray structures. This alignment significantly enhances our confidence in the chosen methodology (Supporting Information Figure S179-S180). The theoretical calculations for the proposed pathway were performed on the super bulky 2b complex. In this context, the reaction of the corresponding cyclic secondary amine, aliphatic aldehyde, and phenylacetylene substrates interacting to form the



Scheme 2. (a). Synthetic route to the monoamine oxidase B inhibitor pargyline through aldehyde:amine:acetylene (A^3) coupling. (b) Gram-scale catalytic reaction of TMS acetylene, HCHO and N-methyl-1-phenylmethanamine with catalyst (**1a**), followed by the treatment of K_2CO_3 to give Pargyline.



Scheme 3. Proposed mechanism the copper (**1–2a**) and the silver (**1–2b**) complexes catalyzed Aldehyde–Amine–Acetylene (A^3) coupling reaction for representative substrate namely morpholine, isobutyraldehyde and phenyl acetylene.

propargylamine product (**5**) by A^3 coupling as mediated by the **2b** complex was studied.

2.3. The ^{13}C NMR chemical shift analysis

For the spectroscopic calculations of ^{13}C NMR, we employed the Orca 5.0 version software [77,78]. The optimized coordinates obtained from DFT calculations served as the input for these computations [66].

These calculations were conducted using the B3LYP hybrid functional [70,71,74] in conjunction with specific basis sets: SARC-ZORA-TZVPP for silver and copper transition metals [79,80], ZORA-def2-TZVP for chlorine (Cl) and bromine (Br) atoms [81], IGLO-II for carbon (C), and (Si) atoms [82,83] and ZORA-def2-SVP for oxygen (O), nitrogen (N), and hydrogen (H) atoms [84]. The identical methodology was also employed for ^{13}C NMR calculations in the case of trimethylsilyl (TMS).

The calculated ^{13}C NMR chemical shifts for the copper (**1–2a**) and

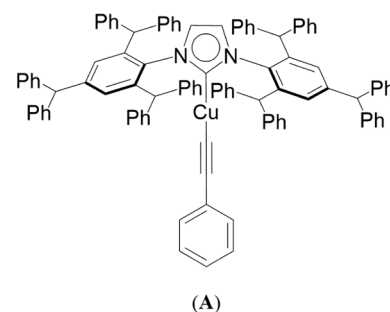
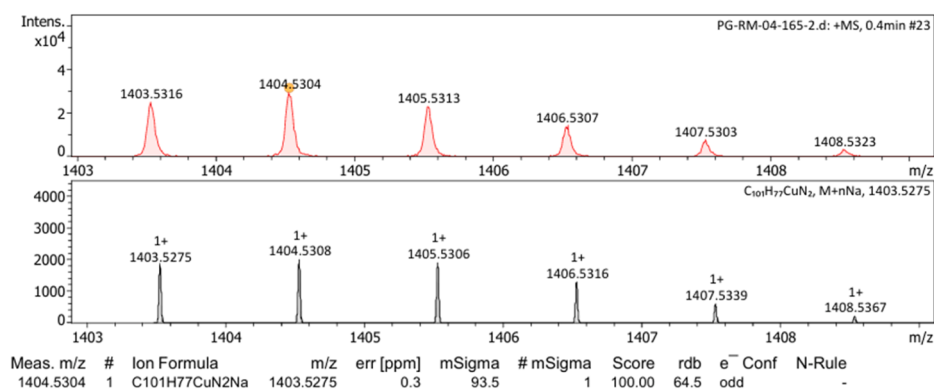


Fig. 5. HRMS spectra of [1,3-{2,4,6-(Ph₂CH)₃C₆H₂}₂-imidazol-2-ylidene]Cu(C≡CPh) (A) detected in the reaction mixture of a 1:1 ratio of phenyl acetylene : morpholine: 1 mol% of **2a**, and 5.0 mL of toluene at room temperature for 15 min. [(a) Experimental and (b) Simulated pattern of ESI-MS data].

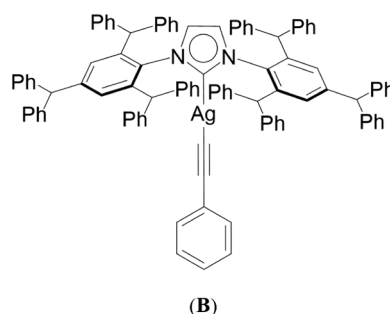
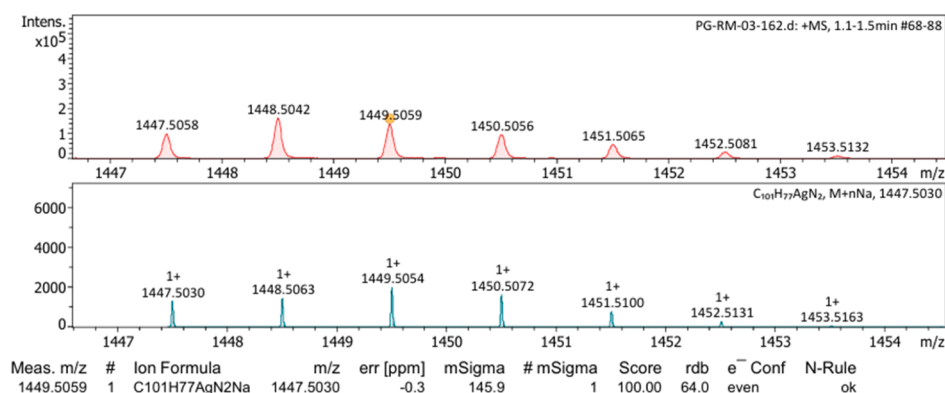


Fig. 6. HRMS spectra of [1,3-{2,4,6-(Ph₂CH)₃C₆H₂}₂-imidazol-2-ylidene]Ag(C≡CPh) (B) detected in the reaction mixture of a 1:1 ratio of phenyl acetylene : morpholine: 1 mol% of **1b**, and 5.0 mL of toluene at room temperature for 15 min. [(a) Experimental and (b) Simulated pattern of ESI-MS data].

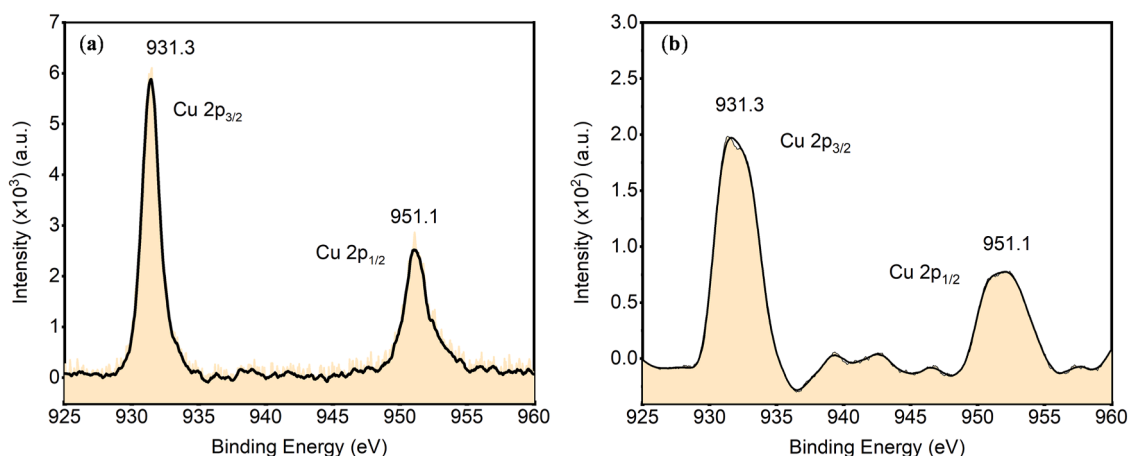


Fig. 7. XPS analysis of the 2p core level peaks of Cu (I), (a) catalyst **2a**, and (b) catalyst **2a** after treatment with phenyl acetylene, morpholine, and isobutyraldehyde for 16 h in 5 mL of toluene at 100 °C.

the silver (**1-2b**) complexes are similar to the experimentally reported values (Supporting Information Table S5). For instance, in the case of the copper (**1-2a**) and the silver (**1-2b**) complexes, the experimentally determined chemical shifts, δ ca. 180.5 ppm for (Cu-N \bar{C} N) peak and δ ca. 184.4 - 184.5 ppm for (Ag-N \bar{C} N) peak, align closely with their respective computed counterparts, δ 192.9 ppm for (Cu-N \bar{C} N) and δ 191.5 - 192.5 ppm for (Ag-N \bar{C} N) (Supporting Information Table S5). These findings align with similar differences between observed and computed chemical shifts reported earlier [39,85–87]. The computed deshielding effects

observed imply that the dominant factor influencing the Cu-N \bar{C} N carbene and (Ag-N \bar{C} N) carbene bonds arises from the σ character of the corresponding occupied molecular orbital. The notable difference of ca. 8–12 ppm observed in our copper (**1-2a**) and the silver (**1-2b**) complexes can be attributed to the paramagnetic spin-orbit term, while the other contributions remain relatively stable, consistent with the previous findings [39,85–87]. Another noteworthy discovery concerns in the copper (**1-2a**) complexes, the difference in chemical shift between the observed and computed values gradually diminishes as you move from

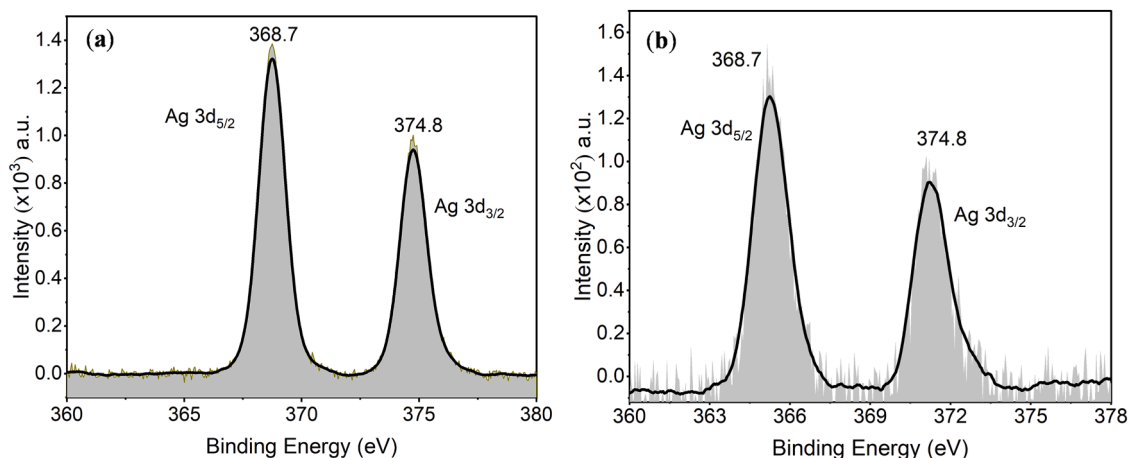


Fig. 8. XPS analysis of the 3d core level peaks of Ag (I), (a) catalyst **2b**, and (b) catalyst **2b** after treatment with phenyl acetylene, morpholine, and isobutyraldehyde for 16 h in 5 mL of toluene at 100 °C.

the deshielding to the shielding region. However, in the case of silver (1–2)**b** complexes, a similar trend can be observed, with the exception of the (Ag–N $\overline{\text{C}}\text{N}$) peak values.

2.4. Steric parameter (% buried volume) analysis

The steric mapping plot, along with the computation of buried volume (% V_{Bur}) for the copper (1–2)**a** and the silver (1–2)**b** complexes, was performed utilizing SambVca 2.0 (A Web Tool for Analysing Catalytic Pockets with Topographic Steric Maps) [88]. The steric mapping plot provides the calculated % V_{Bur} volume, which correlates with the steric factor. This calculated steric mapping plot was generated using the default values within the SambVca 2.0 web tool (Supporting Information Figure S181–S182 for the Cartesian coordinate representation).

Steric map plot and percent buried volume (% V_{Bur}) computations were conducted for copper (1–2)**a** and the silver (1–2)**b** complexes. A comparative analysis was undertaken between these results and those of a previously reported hydrohydrazination catalyst reported [39] (Supporting Information Table S6). A comprehensive analysis of the results demonstrated that the sterically demanding super bulky catalysts, **2a** and **2b**, exhibit substantial buried volumes (% V_{Bur}) of ca. 93.6 % and ca. 93.5 %, respectively. In contrast, the previously synthesized hydrohydrazination catalyst based on gold(I) Acyclic Aminoxy Carbene (AAOC) complexes, which structurally are more relaxed due to the acyclic nature of the singlet carbene ligand, displayed comparatively smaller buried volumes (% V_{Bur}) of ca. 84.9 % – 91.3 %. These findings underscore the critical role of steric effects of the super bulky N-heterocyclic carbene in efficiently governing this catalytic transformation by providing a steric environmental pocket around the catalytically active metal center.

The above % V_{Bur} calculations[89] were performed with the inclusion of hydrogen taking into account the weak van der Waals interactions that prevail between the incoming substrates and the concerned catalysts in the course of catalysis and which more often than not play a significant role in the catalysis trajectory. However, the % V_{Bur} calculation values with the exclusion of hydrogens were obtained for a comparison with the literature reported values that have been done with the exclusion of hydrogens (See Supporting Information Figure S181–S182). For example, a % V_{Bur} of ≈ 68.0 ($r = 5.5 \text{ \AA}$), excluding hydrogens, is reported for a related copper(I) analog[23] that compares well with our current values of ≈ 68.5 % to 68.9 % ($r = 7.0 \text{ \AA}$) (excluding hydrogens). (Supporting Information Figure S183).

2.5. Mechanistic studies

We have performed DFT calculations on a representative **2b** complex (Fig. 9 and Supporting Information Figure S179 and S180), and the mechanism adapted for our calculations is shown in Scheme 3. The reaction begins with the species **2b**, with the phenylacetylene entering the coordination sphere leading to the formation of a reactant complex (RC) wherein the phenylacetylene is anchored to the catalyst *via* a number of non-covalent interactions (NCI) (Supporting Information Figure S184). In the subsequent step, phenylacetylene approaches the Ag center closer, leading to the cleavage of the Ag–Br bond *via* a dissociative mechanism leading to the formation of **Int1** with the silver-bound acetylene complex. In the subsequent stage, a hydrogen transfer event transpires from the phenylacetylene species to the cyclic secondary amine species, mediated *via* the transition state **TS1**. This event leads to the creation of a silver metal-bound acetylide species known as **Int2**, whose presence has been corroborated through mass spectroscopy [1,3- $\{2,4,6-(\text{Ph}_2\text{CH})_3\text{C}_6\text{H}_2\}_2\text{-imidazol-2-ylidene}\}\text{Ag}(\text{C}\equiv\text{CPh})$ (**B**) (Supporting Information Figure S70). In the subsequent stage, the silver-bound acetylide species initiates an attack on the protonated Schiff's base imine during the transition state of C–C coupling. This process results in the formation of the propargylamine product and concurrently regenerates the catalyst (Fig. 9).

The optimized geometries of **2b** display Ag–Br and Ag–C(1) bonds with bond distances of 2.469 Å and 2.102 Å, respectively (Supporting Information Figure S186). The Wiberg Bond Index (WBI) analysis yields values of 0.48 and 0.40 for these respective bonds, indicative of their single-bond character. Further natural bonding orbital (NBO) analysis reveals strong ionic character for these bonds, with more than 80 % of donation arising from the corresponding donor atoms as seen in the $\text{Ag}_{(s)} 13.50\% - \text{Br}_{(pz)} 86.50\%$, and $\text{Ag}_{(s)} 13.43\% - \text{C}(1)_{(pz)} 86.57\%$ values (Supporting Information Figure S185). The formation of the RC is found to be endothermic by 45.1 kJ/mol. At this geometry, the C(1)–Ag–Br angle was found to bend significantly (154.1° *versus* 180.0° in **2b**) and also form rather a strong C–H \cdots Br bond with incoming phenylacetylene and this is also accompanied by a lengthening of the Ag–Br bond with enhanced polarity (more significant negative charge in the Br), setting the stage for its cleavage in the next cycle (Supporting Information Figure S183 and Table S7). In the next step the **Int1** formation occurs with slight endothermicity (+3.7 kJ/mol) and a relaxed scan reveals that this step is a barrier-less process (Fig. 10 and Supporting Information Figure S186). Notably, the bond distances governing the acetylene-silver interaction, along with Ag–C(2) and Ag–C(2 i), were measured at 2.305 and 2.434 Å, respectively (Supporting Information Figure S183). In the subsequent stage, the amine group becomes a key participant, engaging in hydrogen

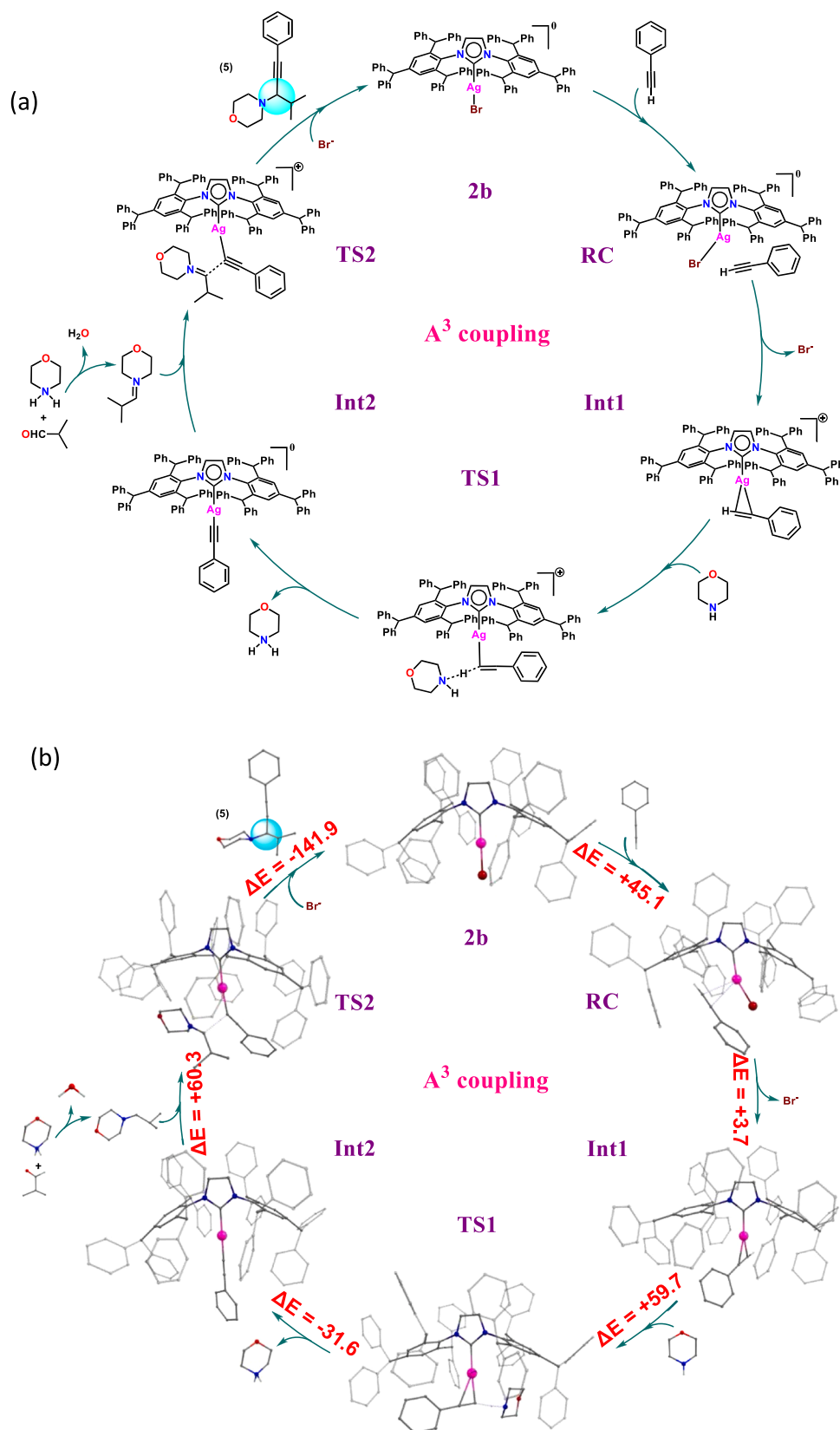


Fig. 9. A proposed mechanism as shown by (a) a simplified Chem Draw illustration and (b) by computed geometries for the A^3 coupling as mediated by **2b**. (Energy in kJ/mol, with Gibbs free energy correction).

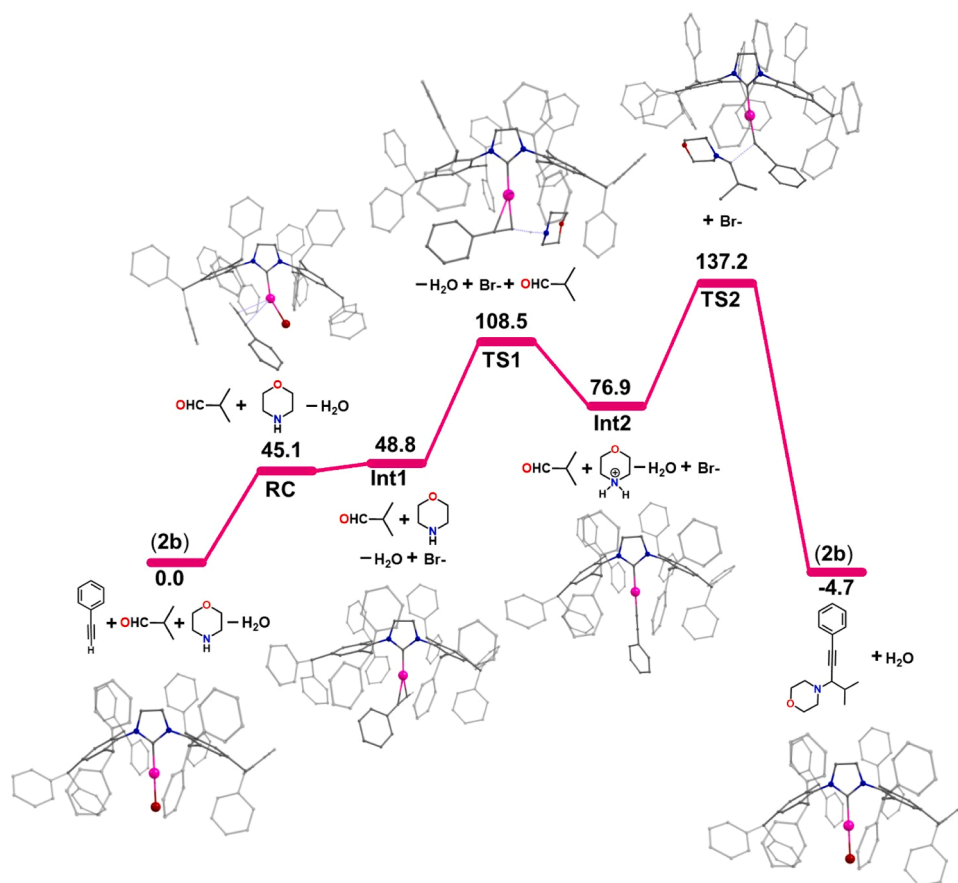


Fig. 10. Energy profile diagram for A^3 coupling as mediated by **2b** is shown. (Energy in kJ/mol, with Gibbs free energy correction).

transfer from the attached acetylene moiety during the transition state (TS1) formation with a barrier of 59.7 kJ/mol. The Ag–C(2') bond is elongated at this transition state by 0.08 Å. The hydrogen transfer from the acetylene C(2)–H(1) bond takes place at a distance of 1.425 Å, while the amine moiety shows this transfer with a H(1)–N(2) bond distance of 1.244 Å (Supporting Information Figure S183). The orbital plot diagram shows the increase in the HOMO-LUMO gap while moving from **Int1** to **TS1**, which signifies the observed high activation energy barrier characteristic of the transition state (Supporting Information Figure S187). Following the hydrogen abstraction by the amine group in the subsequent step, the acetylide-bound silver species (**Int2**) formation ensues. This event, validated through mass spectroscopy, provides an additional layer of confidence in support of the proposed pathway. The formation of the acetylide-bound silver species (**Int2**) is found to be endothermic by 28.8 kJ/mol. Here, the geometric parameters are identified as 2.038 Å for the Ag–C(2) bond and 1.230 Å for the C(2)–C(2') bond. These bond characteristics find additional affirmation through both Wiberg Bond Index (WBI) and Natural Bond Orbital (NBO) analyses (for NBO, and WBI details of all optimized species, (Supporting Information Figure S188-S191 and Table S8). In the subsequent steps of the proposed mechanism, the acetylide species coordinated to silver (**Int2**) takes on the role of a nucleophile and initiates an attack on the protonated Schiff's base imine. This sequential process leads to forming the product propargylamine compound (**5**) and the subsequent catalyst regeneration. The transition state signifies an energy barrier of 60.3 kJ/mol from **Int2**. Although the barrier height is larger, hinting at kinetic hindrance at play, it is important to note the reactions are conducted at elevated temperatures (100 °C), substantiating the manifestation of a high-energy barrier.

This transition state (**TS2**) formation step emphasizes the significance of the C–C coupling step as the rate-determining event in the A^3

coupling reaction. The optimized geometry exposes a C–C coupling distance of 2.271 Å. Notably, during the transition state, a marginal elongation is evident in the Ag–C(2) bond, indicating its readiness to act as a nucleophile and engage in attack. The Wiberg Bond Index (WBI) analysis showcases a value of 0.29 for the C2-C3 bond, subtly suggesting a single bond character. This observation finds further reinforcement through the Natural Bond Orbital (NBO) analysis, which underscores the bonding nature between the C(2)–C(3) bond (C(2)_{(pz)45.13} %–C(3)_{(pz)54.87} %) (Supporting Information Figure S191). When progressing from **Int2** to **TS2**, a noticeable decrease in the HOMO-LUMO gap is observed (Supporting Information Figure S187). This reduction signifies electronic effects that lower the energy gap, thereby facilitating the C–C coupling. Additionally, it is evident that weak interactions (obtained by non-covalent interaction (NCI) analysis), such as van der Waals forces (C–H...π, π...π, C–H...O) (Supporting Information Figure S192), play a significant role in anchoring the Schiff's base imine in the vicinity during the formation of the transition state (**TS2**). To elucidate the cause of the relatively high barrier computed for **TS2**, we conducted a deformation energy analysis, revealing an energy penalty of 385.8 kJ/mol. This analysis provides a rationale for the estimated barrier (Fig. 10). However, favourable orbital interactions accompanied by a number of non-covalent interactions help to bring down the barrier to 137.2 kJ/mol to make the reaction facile at 100 °C as observed experimentally (Fig. 10 and Supporting Information Figure S192). Subsequently, in the subsequent step, catalyst regeneration occurs as an exothermic process, underscoring the feasibility of the reaction (Fig. 10).

3. Conclusions

In summary, a series of super bulky N-heterocyclic carbene complexes of silver and copper namely, [1,3-{2,4,6-(Ph₂CH)₃C₆H₂}]₂-

imidazol-2-ylidene]MX [where, M = Cu; X = Cl (**1a**), Br (**2a**): M = Ag; X = Cl (**1b**), Br (**2b**)] were synthesized which efficiently carried out the A³ coupling of the secondary amine, aliphatic aldehyde, and phenylacetylene substrates, yielding propargylamine in moderate to good (ca. 65–89 %) yields. Mechanistic investigations based on mass spectrometry studies suggest that the A³ coupling proceeds via a metal bound acetylide species, [1,3-{2,4,6-(Ph₂CH)₃C₆H₂}-imidazol-2-ylidene]M (C≡CPh) [where, M = Cu (**A**), Ag (**B**)]. The DFT investigation further supports that the catalytic cycle begins with species **2b**, leading to the formation of a reactant complex (**RC**) where acetylene binds through non-covalent interactions and shows how weak interactions play an important role during the catalysis. A hydrogen transfer event from phenylacetylene to the cyclic secondary amine species, mediated via transition state **TS1**, follows, creating an acetylide-bound silver species known as **Int2**, confirmed by mass spectroscopy. **Int2** initiates an attack on the protonated Schiff's base imine during the C–C coupling transition state, yielding the catalysis product and regenerating the catalyst with an energy barrier of 60.3 kJ/mol from **Int2** and can be observed as a rate-determining step. In subsequent steps, the acetylide species, coordinated to silver, acts as a nucleophile and initiates an attack on the protonated Schiff's base imine, forming morpholine and regenerating the catalyst. Progressing from **Int2** to **TS2**, a noticeable decrease in the HOMO-LUMO gap occurs, facilitating the C–C coupling state. Weak interactions, including van der Waals forces, significantly stabilize the Schiff's base imine during the formation of transition state **TS2**, collectively contributing to the C–C coupling transition state. The process concludes with an exothermic catalyst regeneration, confirming the A³ coupling reaction's feasibility. The combined experimental and computational study further establishes the favourable influence of the sterically demanding super bulky N-heterocyclic carbenes in the A³ coupling catalysis. The coupling reaction was not only successfully employed for the synthesis of a drug, pargyline, an inhibitor of monoamine oxidase B (MAO-B), but the same was demonstrated for a gram-scale synthesis for a representative catalyst (**1a**). It would pave the way for future research on developing the favourable influence of super bulky N-heterocyclic carbene ligands on catalysis.

4. Experimental section

General procedures: All manipulations were carried out using a combination of a glovebox and standard Schlenk techniques. Solvents were purified and degassed by standard procedures. Ag₂O was purchased from Spectrochem Pvt. Ltd, and Cu₂O from Aldrich. 2,4,6-tribenzylhydrylaniline[17] was synthesised according to literature procedure. The compound [1,3-{2,4,6-(Ph₂CH)₃C₆H₂}-imidazolium]Cl (**1**) was synthesised by modified procedure than that reported in the literature[17,23] and [1,3-{2,4,6-(Ph₂CH)₃C₆H₂}-imidazol-2-ylidene]CuCl (**1a**) was synthesised by different procedure than that reported in the literature [23]. ¹H NMR, ¹³C{¹H} NMR, spectra were recorded on Bruker 400 & 500 MHz spectrometer. ¹H NMR peaks are labelled as singlet (s), doublet (d), triplet (t), doublet of doublet (dd) and multiplet (m). Infrared spectra were recorded on a Perkin Elmer Spectrum One FT-IR spectrometer. Mass spectrometry measurements were done on a Micromass Q-ToF spectrometer and Bruker maxis impact spectrometer. Elemental analysis was carried out on ThermoFinnigan FLASH EA 1112 SERIES (CHNS) Elemental analyser. X-ray photoelectron spectra were acquired on Kartos analytical AXIS Supra spectrometer with a monochromatic Al K α X-ray source (1486.6 eV) using a pass energy of 20 eV. The XPS binding energies were referred to the C 1s peak at 284.6 eV [90], to give an accurate energy calibration. X-ray diffraction data for compounds **1b**, **2a** and **2b** were collected on a Bruker APEX 2 CCD platform diffractometer (MoK α (k = 0.71073 Å)) equipped with an Oxford liquid nitrogen cryostream. Crystals were mounted in a nylon loop with Paratone-N cryoprotectant oil. The structures were solved using direct methods and standard difference map techniques, and were refined by full-matrix least-squares procedures on *F*² with SHELXTL

(Version 6.14) [91]. CCDC-2218967 (for **1b**), CCDC-2218671 (for **2a**), and CCDC-2218670 (for **2b**), contain the supplementary crystallographic data related to this article. These data can be obtained free of charge from the Cambridge Crystallographic Data center via www.ccdc.cam.ac.uk/data_request/cif.

[1,3-{2,4,6-(Ph₂CH)₃C₆H₂}-imidazolium] Cl (**1**) [17,23]

To a solution of 2,4,6-tribenzylhydrylaniline (2.00 g, 3.40 mmol) in CH₂Cl₂ (ca. 40 mL), 40 % aqueous glyoxal (0.993 g, 6.85 mmol) was added and stirred for 45 min. To this reaction mixture, 37 % aqueous formaldehyde (1.40 g, 17.2 mmol) and HCl (ca. 2 mL) were added and stirred for 24 h at 45 °C, after which the volatiles were removed under reduced pressure. The black material was extracted with CHCl₃ (ca. 2 × 10 mL) and dried over anhydrous Na₂SO₄. Then the resulting crude compound was purified by column chromatography in silica gel using CHCl₃:CH₃OH (95:5 v/v) to give the product as brown colour solid (1.14 g 27 %). ¹H NMR (CDCl₃, 400 MHz, 25 °C): δ ppm 13.0 (s, 1H, NCHN), 7.18–7.06 (m, 44H, 2C₆H₂(CH(C₆H₅)₂)₃), 6.92 (d, 8H, J_{H-H} = 8 Hz, 2C₆H₂(CH(C₆H₅)₂)₃), 6.71 (s, 4H, 2C₆H₂(CH(C₆H₅)₂)₃), 6.70 (d, 8H, J_{H-H} = 8 Hz, 2C₆H₂(CH(C₆H₅)₂)₃), 5.61 (s, 2H, NC₂H₂N), 5.35 (s, 2H, 2C₆H₂(CH(C₆H₅)₂)₃), 5.27 (s, 4H, 2C₆H₂(CH(C₆H₅)₂)₃). ¹³C{¹H} NMR (CDCl₃, 100 MHz, 25 °C): δ 147.2 (NCHN), 142.6 (C₆H₂(CH(C₆H₅)₂)₃), 142.1 (2C₆H₂(CH(C₆H₅)₂)₃), 141.6 (2C₆H₂(CH(C₆H₅)₂)₃), 140.5 (2C₆H₂(CH(C₆H₅)₂)₃), 131.5 (2C₆H₂(CH(C₆H₅)₂)₃), 130.3 (2C₆H₂(CH(C₆H₅)₂)₃), 129.7 (2C₆H₂(CH(C₆H₅)₂)₃), 129.2 (2C₆H₂(CH(C₆H₅)₂)₃), 129.0 (2C₆H₂(CH(C₆H₅)₂)₃), 128.6 (2C₆H₂(CH(C₆H₅)₂)₃), 128.5 (2C₆H₂(CH(C₆H₅)₂)₃), 128.3 (2C₆H₂(CH(C₆H₅)₂)₃), 126.9 (2C₆H₂(CH(C₆H₅)₂)₃), 126.7 (2C₆H₂(CH(C₆H₅)₂)₃), 126.4 (2C₆H₂(CH(C₆H₅)₂)₃), 123.5 (NC₂H₂N), 56.1 (2C₆H₂(CH(C₆H₅)₂)₃), 51.4 (2C₆H₂(CH(C₆H₅)₂)₃). IR data (cm⁻¹) KBr pellet: 3057 (m), 3027 (m), 2905 (s), 2755 (w), 1952 (w), 1814 (w), 1598 (m), 1523 (m), 1493 (s), 1446 (s), 1269 (w), 1142 (w), 1079 (m), 1029 (s), 918 (w), 848 (w), 766 (m), 747 (m), 705 (s), 606 (w), 517 (w). HRMS (ESI) *m/z* 1217.5773 [C₉₃H₇₃N₂-Cl]⁺ calcd 1217.5768. Anal. Calcd. for C₉₃H₇₃ClN₂: C, 89.07; H, 5.87; N, 2.23. Found: C, 87.18; H, 5.54; N, 3.83 %.

[1,3-{2,4,6-(Ph₂CH)₃C₆H₂}-imidazol-2-ylidene] CuCl (**1a**) [23]

To a solution of [1,3-{2,4,6-(Ph₂CH)₃C₆H₂}-imidazolium]Cl (**1**) (1.501 g, 1.20 mmol) in CH₂Cl₂ (ca. 20 mL), Cu₂O (0.501 g, 3.50 mmol) was added and stirred in dark at room temperature for 12 h. The resulting reaction mixture was filtered over celite, and washed with CH₂Cl₂ (ca. 3 × 10 mL). The combined filtrates were collected, and volatiles were removed in *vacuo* to give the product as a white solid. This crude compound was purified by column in neutral alumina using CHCl₃ to get the product as brown solid (**1a**) (0.581 g, 37 %). ¹H NMR (CDCl₃, 400 MHz, 25 °C): δ ppm 7.21–7.07 (m, 36H, 2C₆H₂(CH(C₆H₅)₂)₃), 6.94–6.92 (m, 9H, 2C₆H₂(CH(C₆H₅)₂)₃), 6.89–6.87 (m, 7H, 2C₆H₂(CH(C₆H₅)₂)₃), 6.80–6.78 (m, 12H, 2C₆H₂(CH(C₆H₅)₂)₃ and 2C₆H₂(CH(C₆H₅)₂)₃), 5.91 (s, 2H, NC₂H₂N), 5.39 (s, 2H, 2C₆H₂(CH(C₆H₅)₂)₃), 5.17 (s, 4H, 2C₆H₂(CH(C₆H₅)₂)₃). ¹³C{¹H} NMR (CDCl₃, 100 MHz, 25 °C): δ 180.5 (Cu-NCN), 145.8 (2C₆H₂(CH(C₆H₅)₂)₃), 143.1 (2C₆H₂(CH(C₆H₅)₂)₃), 143.0 (2C₆H₂(CH(C₆H₅)₂)₃), 142.1 (2C₆H₂(CH(C₆H₅)₂)₃), 141.0 (2C₆H₂(CH(C₆H₅)₂)₃), 134.7 (2C₆H₂(CH(C₆H₅)₂)₃), 130.8 (2C₆H₂(CH(C₆H₅)₂)₃), 129.4 (2C₆H₂(CH(C₆H₅)₂)₃), 129.3 (2C₆H₂(CH(C₆H₅)₂)₃), 128.6 (2C₆H₂(CH(C₆H₅)₂)₃), 128.4 (2C₆H₂(CH(C₆H₅)₂)₃), 128.3 (2C₆H₂(CH(C₆H₅)₂)₃), 126.6 (2C₆H₂(CH(C₆H₅)₂)₃), 126.5 (2C₆H₂(CH(C₆H₅)₂)₃), 126.3 (2C₆H₂(CH(C₆H₅)₂)₃), 123.2 (NC₂H₂N), 56.3 (2C₆H₂(CH(C₆H₅)₂)₃), 51.4 (2C₆H₂(CH(C₆H₅)₂)₃). IR data (cm⁻¹) KBr pellet: 3057 (m), 3025 (m), 2923 (w), 1598 (m), 1526 (m), 1493 (s), 1466 (m), 1448 (s), 1283 (w), 1078 (m), 1030 (s), 916 (w), 848 (w), 766 (m), 745 (m), 703 (s), 606 (w), 522 (w). HRMS (ESI) found *m/z* 1280.5023 [C₉₃H₇₃N₂Cu-Cl]⁺ calcd 1280.5019. Anal. Calcd. for C₉₃H₇₃N₂CuCl: C, 84.84; H, 5.51; N, 2.13. Found: C, 85.75; H, 5.17; N, 1.41 %.

[1,3-{2,4,6-(Ph₂CH)₃C₆H₂}-imidazol-2-ylidene] AgCl (**1b**)

To a solution of [1,3-{2,4,6-(Ph₂CH)₃C₆H₂}-imidazolium]Cl (**1**) (0.501 g, 0.40 mmol) in CH₂Cl₂ (ca. 20 mL), Ag₂O (0.151 g, 0.65 mmol) was added and stirred in the dark at room temperature for 12 h. The

resulting reaction mixture was filtered over celite, and washed with CH_2Cl_2 (ca. 3×10 mL). The combined filtrates were collected, and the volatiles were removed in *vacuo* to give the product as a white solid. This crude compound was purified by column in neutral alumina in CHCl_3 to give the product (**1b**) as a solid (0.151 g, 28 %). Single crystals for X-ray diffraction studies were grown from the CHCl_3 employing a slow evaporation technique. ^1H NMR (CDCl_3 , 400 MHz, 25 °C): δ ppm 7.24–7.14 (m, 25H, $2\text{C}_6\text{H}_2(\text{CH}(\text{C}_6\text{H}_5)_2)_3$), 7.11–7.10 (m, 11H, $2\text{C}_6\text{H}_2(\text{CH}(\text{C}_6\text{H}_5)_2)_3$), 6.97–6.96 (d, 8H, $J_{\text{H-H}} = 8$ Hz, $2\text{C}_6\text{H}_2(\text{CH}(\text{C}_6\text{H}_5)_2)_3$), 6.84–6.80 (m, 20H, $2\text{C}_6\text{H}_2(\text{CH}(\text{C}_6\text{H}_5)_2)_3$ and $2\text{C}_6\text{H}_2(\text{CH}(\text{C}_6\text{H}_5)_2)_3$), 6.05 (d, 2H, $\text{NC}_2\text{H}_2\text{N}$), 5.42 (s, 2H, $2\text{C}_6\text{H}_2(\text{CH}(\text{C}_6\text{H}_5)_2)_3$), 5.12 (s, 2H, $4\text{C}_6\text{H}_2(\text{CH}(\text{C}_6\text{H}_5)_2)_3$). $^{13}\text{C}\{^1\text{H}\}$ NMR (CDCl_3 , 100 MHz, 25 °C): δ 184.4 (d, $^1J^{109}\text{Ag}-^{13}\text{C}_{\text{carbene}} = 267$ Hz, $^1J^{107}\text{Ag}-^{13}\text{C}_{\text{carbene}} = 230$ Hz, Ag-NCN), 145.8 ($2\text{C}_6\text{H}_2(\text{CH}(\text{C}_6\text{H}_5)_2)_3$), 143.0 ($2\text{C}_6\text{H}_2(\text{CH}(\text{C}_6\text{H}_5)_2)_3$), 142.9 ($2\text{C}_6\text{H}_2(\text{CH}(\text{C}_6\text{H}_5)_2)_3$), 141.8 ($2\text{C}_6\text{H}_2(\text{CH}(\text{C}_6\text{H}_5)_2)_3$), 140.8 ($2\text{C}_6\text{H}_2(\text{CH}(\text{C}_6\text{H}_5)_2)_3$), 134.7 ($2\text{C}_6\text{H}_2(\text{CH}(\text{C}_6\text{H}_5)_2)_3$), 130.8 ($2\text{C}_6\text{H}_2(\text{CH}(\text{C}_6\text{H}_5)_2)_3$), 129.3 ($2\text{C}_6\text{H}_2(\text{CH}(\text{C}_6\text{H}_5)_2)_3$), 129.2 ($2\text{C}_6\text{H}_2(\text{CH}(\text{C}_6\text{H}_5)_2)_3$), 128.7 ($2\text{C}_6\text{H}_2(\text{CH}(\text{C}_6\text{H}_5)_2)_3$), 128.4 ($2\text{C}_6\text{H}_2(\text{CH}(\text{C}_6\text{H}_5)_2)_3$), 128.3 ($2\text{C}_6\text{H}_2(\text{CH}(\text{C}_6\text{H}_5)_2)_3$), 126.7 ($2\text{C}_6\text{H}_2(\text{CH}(\text{C}_6\text{H}_5)_2)_3$), 126.6 ($2\text{C}_6\text{H}_2(\text{CH}(\text{C}_6\text{H}_5)_2)_3$), 126.4 ($2\text{C}_6\text{H}_2(\text{CH}(\text{C}_6\text{H}_5)_2)_3$), 123.6 ($\text{NC}_2\text{H}_2\text{N}$), 123.5 ($\text{NC}_2\text{H}_2\text{N}$), 56.1 ($2\text{C}_6\text{H}_2(\text{CH}(\text{C}_6\text{H}_5)_2)_3$), 51.2 ($2\text{C}_6\text{H}_2(\text{CH}(\text{C}_6\text{H}_5)_2)_3$). IR data (cm^{-1}) KBr pellet: 3058 (m), 3025 (m), 2922 (w), 1598 (m), 1493 (s), 1467 (m), 1448 (s), 1266 (w), 1078 (m), 1030 (s), 912 (w), 766 (m), 745 (m), 701 (s), 606 (w), 523 (w). HRMS (ESI) found m/z 1325.4763 [$\text{C}_{93}\text{H}_{72}\text{N}_2\text{Ag-Cl}^-$] calcd 1325.4763. Anal. Calcd. for $\text{C}_{93}\text{H}_{72}\text{N}_2\text{AgCl}$: C, 82.08; H, 5.33; N, 2.06. Found: C, 81.21; H, 4.68; N, 1.84 %.

[1,3-{2,4,6-(Ph₂CH)₃C₆H₂}₂-imidazolium] Br (2)

To a solution of 2,4,6-tribenzhydrylaniline (2.00 g, 3.38 mmol) in CH_2Cl_2 (ca. 40 mL), 40 % aqueous glyoxal (0.992, 6.84 mmol) was added and stirred for 45 minutes. To this reaction mixture, 37 % aqueous formaldehyde (1.38 g, 17.04 mmol) and HBr (ca. 2 mL) were added and stirred at 45 °C for 24 h the volatiles were removed under reduced pressure. The black material was extracted with CHCl_3 (ca. 2×10 mL) and dried over anhydrous Na_2SO_4 . Then the resulting crude compound was purified by column chromatography in silica gel using $\text{CHCl}_3:\text{CH}_3\text{OH}$ (95:5 v/v) to give the product as brown colour solid (0.714 g, 16 %). ^1H NMR (CDCl_3 , 400 MHz, 25 °C): δ ppm 12.39 (s, 1H, NCHN), 7.20–7.13 (m, 44H, $2\text{C}_6\text{H}_2(\text{CH}(\text{C}_6\text{H}_5)_2)_3$), 6.96 (d, 8H, $J_{\text{H-H}} = 8$ Hz, $2\text{C}_6\text{H}_2(\text{CH}(\text{C}_6\text{H}_5)_2)_3$), 6.79–6.74 (m, 12H, $2\text{C}_6\text{H}_2(\text{CH}(\text{C}_6\text{H}_5)_2)_3$ and $2\text{C}_6\text{H}_2(\text{CH}(\text{C}_6\text{H}_5)_2)_3$), 5.75 (s, 2H, $\text{NC}_2\text{H}_2\text{N}$), 5.39 (s, 2H, $2\text{C}_6\text{H}_2(\text{CH}(\text{C}_6\text{H}_5)_2)_3$), 5.28 (s, 4H, $2\text{C}_6\text{H}_2(\text{CH}(\text{C}_6\text{H}_5)_2)_3$). $^{13}\text{C}\{^1\text{H}\}$ NMR (CDCl_3 , 100 MHz, 25 °C): δ 147.3 (NCHN), 142.6 ($2\text{C}_6\text{H}_2(\text{CH}(\text{C}_6\text{H}_5)_2)_3$), 142.1 ($2\text{C}_6\text{H}_2(\text{CH}(\text{C}_6\text{H}_5)_2)_3$), 141.6 ($2\text{C}_6\text{H}_2(\text{CH}(\text{C}_6\text{H}_5)_2)_3$), 140.5 ($2\text{C}_6\text{H}_2(\text{CH}(\text{C}_6\text{H}_5)_2)_3$), 131.5 ($2\text{C}_6\text{H}_2(\text{CH}(\text{C}_6\text{H}_5)_2)_3$), 130.3 ($2\text{C}_6\text{H}_2(\text{CH}(\text{C}_6\text{H}_5)_2)_3$), 129.8 ($2\text{C}_6\text{H}_2(\text{CH}(\text{C}_6\text{H}_5)_2)_3$), 129.2 ($2\text{C}_6\text{H}_2(\text{CH}(\text{C}_6\text{H}_5)_2)_3$), 129.1 ($2\text{C}_6\text{H}_2(\text{CH}(\text{C}_6\text{H}_5)_2)_3$), 128.7 ($2\text{C}_6\text{H}_2(\text{CH}(\text{C}_6\text{H}_5)_2)_3$), 128.5 ($2\text{C}_6\text{H}_2(\text{CH}(\text{C}_6\text{H}_5)_2)_3$), 128.4 ($2\text{C}_6\text{H}_2(\text{CH}(\text{C}_6\text{H}_5)_2)_3$), 127.1 ($2\text{C}_6\text{H}_2(\text{CH}(\text{C}_6\text{H}_5)_2)_3$), 126.8 ($2\text{C}_6\text{H}_2(\text{CH}(\text{C}_6\text{H}_5)_2)_3$), 126.4 ($2\text{C}_6\text{H}_2(\text{CH}(\text{C}_6\text{H}_5)_2)_3$), 123.7 ($\text{NC}_2\text{H}_2\text{N}$), 56.2 ($2\text{C}_6\text{H}_2(\text{CH}(\text{C}_6\text{H}_5)_2)_3$), 51.4 ($2\text{C}_6\text{H}_2(\text{CH}(\text{C}_6\text{H}_5)_2)_3$). IR data (cm^{-1}) KBr pellet: 3416 (w), 3058 (m), 3026 (m), 2876 (s), 2755 (w), 1598 (m), 1526 (m), 1493 (s), 1447 (s), 1256 (w), 1140 (w), 1079 (m), 1030 (s), 916 (w), 848 (w), 766 (m), 746 (m), 703 (s), 606 (w), 518 (w). HRMS (ESI) m/z found 1218.5807 [$\text{C}_{93}\text{H}_{73}\text{N}_2\text{-Br}^+$] calcd 1218.5802. Anal. Calcd. for $\text{C}_{93}\text{H}_{73}\text{BrN}_2$: C, 86.02; H, 5.67; N, 2.16. Found: C, 85.33; H, 5.65; N, 2.56 %.

[1,3-{2,4,6-(Ph₂CH)₃C₆H₂}₂-imidazol-2-ylidene] CuBr (2a)

To the solution of [1,3-{2,4,6-(Ph₂CH)₃C₆H₂}₂-imidazolium] Br (2) (1.01 g, 0.782 mmol) in CH_2Cl_2 (ca. 20 mL), Cu_2O (0.257 g, 1.79 mmol) was added and stirred in the dark at room temperature for 12 hours. The resulting reaction mixture was filtered over celite, and washed with CH_2Cl_2 (ca. 3×10 mL). The combined filtrates were collected, and the volatiles were removed in *vacuo* to give the product as a white solid. This crude compound was purified by column in neutral alumina in CHCl_3 to give the product (**2a**) as a solid (0.310 g, 29 %). Single crystals for X-ray diffraction studies were grown from the CHCl_3 employing a

slow evaporation technique. ^1H NMR (CDCl_3 , 400 MHz, 25 °C): δ ppm 7.23–7.07 (m, 36H, $2\text{C}_6\text{H}_2(\text{CH}(\text{C}_6\text{H}_5)_2)_3$), 6.92 (d, 10H, $J_{\text{H-H}} = 8$ Hz, $2\text{C}_6\text{H}_2(\text{CH}(\text{C}_6\text{H}_5)_2)_3$), 6.88–6.86 (m, 8H, $2\text{C}_6\text{H}_2(\text{CH}(\text{C}_6\text{H}_5)_2)_3$), 6.80–6.77 (m, 10H, $2\text{C}_6\text{H}_2(\text{CH}(\text{C}_6\text{H}_5)_2)_3$ and $2\text{C}_6\text{H}_2(\text{CH}(\text{C}_6\text{H}_5)_2)_3$), 5.91 (s, 2H, $\text{NC}_2\text{H}_2\text{N}$), 5.39 (s, 2H, $2\text{C}_6\text{H}_2(\text{CH}(\text{C}_6\text{H}_5)_2)_3$), 5.16 (s, 4H, $2\text{C}_6\text{H}_2(\text{CH}(\text{C}_6\text{H}_5)_2)_3$). $^{13}\text{C}\{^1\text{H}\}$ NMR (CDCl_3 , 100 MHz, 25 °C): δ 180.5 (Cu-NCN), 145.7 ($2\text{C}_6\text{H}_2(\text{CH}(\text{C}_6\text{H}_5)_2)_3$), 143.1 ($2\text{C}_6\text{H}_2(\text{CH}(\text{C}_6\text{H}_5)_2)_3$), 142.9 ($2\text{C}_6\text{H}_2(\text{CH}(\text{C}_6\text{H}_5)_2)_3$), 142.1 ($2\text{C}_6\text{H}_2(\text{CH}(\text{C}_6\text{H}_5)_2)_3$), 140.9 ($2\text{C}_6\text{H}_2(\text{CH}(\text{C}_6\text{H}_5)_2)_3$), 134.6 ($2\text{C}_6\text{H}_2(\text{CH}(\text{C}_6\text{H}_5)_2)_3$), 130.8 ($2\text{C}_6\text{H}_2(\text{CH}(\text{C}_6\text{H}_5)_2)_3$), 129.4 ($2\text{C}_6\text{H}_2(\text{CH}(\text{C}_6\text{H}_5)_2)_3$), 129.3 ($2\text{C}_6\text{H}_2(\text{CH}(\text{C}_6\text{H}_5)_2)_3$), 129.2 ($2\text{C}_6\text{H}_2(\text{CH}(\text{C}_6\text{H}_5)_2)_3$), 128.5 ($2\text{C}_6\text{H}_2(\text{CH}(\text{C}_6\text{H}_5)_2)_3$), 128.4 ($2\text{C}_6\text{H}_2(\text{CH}(\text{C}_6\text{H}_5)_2)_3$), 128.3 ($2\text{C}_6\text{H}_2(\text{CH}(\text{C}_6\text{H}_5)_2)_3$), 128.1 ($2\text{C}_6\text{H}_2(\text{CH}(\text{C}_6\text{H}_5)_2)_3$), 126.6 ($2\text{C}_6\text{H}_2(\text{CH}(\text{C}_6\text{H}_5)_2)_3$), 126.5 ($2\text{C}_6\text{H}_2(\text{CH}(\text{C}_6\text{H}_5)_2)_3$), 126.3 ($2\text{C}_6\text{H}_2(\text{CH}(\text{C}_6\text{H}_5)_2)_3$), 123.2 ($\text{NC}_2\text{H}_2\text{N}$), 56.2 ($2\text{C}_6\text{H}_2(\text{CH}(\text{C}_6\text{H}_5)_2)_3$), 51.3 ($2\text{C}_6\text{H}_2(\text{CH}(\text{C}_6\text{H}_5)_2)_3$). IR data (cm^{-1}) KBr pellet: 3057 (m), 3025 (m), 2921 (w), 1598 (m), 1493 (s), 1466 (m), 1448 (s), 1283 (w), 1078 (m), 1030 (m), 916 (w), 766 (m), 745 (m), 703 (s), 606 (w), 522 (w). HRMS (ESI) m/z found 1280.5023 [$\text{C}_{93}\text{H}_{72}\text{N}_2\text{Cu-Br}^+$] calcd 1280.5019. Anal. Calcd. for $\text{C}_{93}\text{H}_{72}\text{N}_2\text{CuBr}$: C, 82.07; H, 5.33; N, 2.06. Found: C, 82.67; H, 5.48; N, 2.43 %.

[1,3-{2,4,6-(Ph₂CH)₃C₆H₂}₂-imidazol-2-ylidene] AgBr (2b)

To the solution of [1,3-{2,4,6-(Ph₂CH)₃C₆H₂}₂-imidazolium] Br (2) (1.07 g, 0.824 mmol) in CH_2Cl_2 (ca. 20 mL), Ag_2O (0.315 g, 1.35 mmol) was added stirred in the dark at room temperature for 12 hours. The resulting reaction mixture was filtered over celite, and washed with CH_2Cl_2 (ca. 3×10 mL). The combined filtrates were collected, and the volatiles were removed in *vacuo* to give the product as a white solid. This crude compound was purified by column in neutral alumina in CHCl_3 to give the product (**2b**) as a solid (0.232 g, 20 %). Single crystals for X-ray diffraction studies were grown from the CHCl_3 employing a slow evaporation technique. ^1H NMR (CDCl_3 , 400 MHz, 25 °C): δ ppm 7.21–7.12 (m, 24H, $2\text{C}_6\text{H}_2(\text{CH}(\text{C}_6\text{H}_5)_2)_3$), 7.09–7.07 (m, 12H, $2\text{C}_6\text{H}_2(\text{CH}(\text{C}_6\text{H}_5)_2)_3$), 6.93 (d, 8H, $2\text{C}_6\text{H}_2(\text{CH}(\text{C}_6\text{H}_5)_2)_3$), 6.80–6.77 (m, 20H, $2\text{C}_6\text{H}_2(\text{CH}(\text{C}_6\text{H}_5)_2)_3$ and $2\text{C}_6\text{H}_2(\text{CH}(\text{C}_6\text{H}_5)_2)_3$), 6.04 (s, 2H, $\text{NC}_2\text{H}_2\text{N}$), 5.40 (s, 2H, $2\text{C}_6\text{H}_2(\text{CH}(\text{C}_6\text{H}_5)_2)_3$), 5.08 (s, 4H, $2\text{C}_6\text{H}_2(\text{CH}(\text{C}_6\text{H}_5)_2)_3$). $^{13}\text{C}\{^1\text{H}\}$ NMR (CDCl_3 , 100 MHz, 25 °C): δ 184.5 (d, $^1J^{109}\text{Ag}-^{13}\text{C}_{\text{carbene}} = 267$ Hz, $^1J^{107}\text{Ag}-^{13}\text{C}_{\text{carbene}} = 231$ Hz, Ag-NCN), 145.9 ($2\text{C}_6\text{H}_2(\text{CH}(\text{C}_6\text{H}_5)_2)_3$), 143.0 ($2\text{C}_6\text{H}_2(\text{CH}(\text{C}_6\text{H}_5)_2)_3$), 142.9 ($2\text{C}_6\text{H}_2(\text{CH}(\text{C}_6\text{H}_5)_2)_3$), 141.8 ($2\text{C}_6\text{H}_2(\text{CH}(\text{C}_6\text{H}_5)_2)_3$), 140.8 ($2\text{C}_6\text{H}_2(\text{CH}(\text{C}_6\text{H}_5)_2)_3$), 134.8 ($2\text{C}_6\text{H}_2(\text{CH}(\text{C}_6\text{H}_5)_2)_3$), 130.9 ($2\text{C}_6\text{H}_2(\text{CH}(\text{C}_6\text{H}_5)_2)_3$), 129.2 ($2\text{C}_6\text{H}_2(\text{CH}(\text{C}_6\text{H}_5)_2)_3$), 128.7 ($2\text{C}_6\text{H}_2(\text{CH}(\text{C}_6\text{H}_5)_2)_3$), 128.5 ($2\text{C}_6\text{H}_2(\text{CH}(\text{C}_6\text{H}_5)_2)_3$), 128.4 ($2\text{C}_6\text{H}_2(\text{CH}(\text{C}_6\text{H}_5)_2)_3$), 126.7 ($2\text{C}_6\text{H}_2(\text{CH}(\text{C}_6\text{H}_5)_2)_3$), 126.6 ($2\text{C}_6\text{H}_2(\text{CH}(\text{C}_6\text{H}_5)_2)_3$), 126.4 ($2\text{C}_6\text{H}_2(\text{CH}(\text{C}_6\text{H}_5)_2)_3$), 123.7 ($\text{NC}_2\text{H}_2\text{N}$), 123.6 ($\text{NC}_2\text{H}_2\text{N}$), 56.2 ($2\text{C}_6\text{H}_2(\text{CH}(\text{C}_6\text{H}_5)_2)_3$), 51.3 ($2\text{C}_6\text{H}_2(\text{CH}(\text{C}_6\text{H}_5)_2)_3$). IR data (cm^{-1}) KBr pellet: 3058 (m), 3025 (m), 2922 (w), 1598 (m), 1493 (s), 1467 (m), 1448 (s), 1384 (w), 1266 (w), 1078 (m), 1030 (m), 915 (w), 766 (m), 745 (m), 701 (s), 606 (w), 523 (w). LRMS (ESI) m/z found 1325 [$\text{C}_{93}\text{H}_{72}\text{N}_2\text{Ag-Br}^+$] calcd 1325. Anal. Calcd. for $\text{C}_{93}\text{H}_{72}\text{N}_2\text{AgBr}$: C, 79.48; H, 5.16; N, 1.99. Found: C, 78.89; H, 5.20; N, 2.00 %.

General procedure for Aldehyde–Amine–Acetylene (A³) coupling reaction for synthesis of propargylamine.

In a typical catalysis run, calculated amount of metal–NHC precatalyst **1a/1b/2a/2b** (0.02 mmol, 1 mol %) was dissolved in 5 mL of toluene and to this solution phenyl acetylene (2.00 mmol) was added and stirred for 15 minutes followed by addition of aldehyde (2.00 mmol) and amine (2.00 mmol) in the respective order and was stirred at 100 °C for 16 hours. The reaction was quenched with Et_2O , extracted with ca. 2×10 mL of CH_2Cl_2 , the combined organic fraction was dried over Na_2SO_4 , and the volatiles were removed under reduced pressure to obtain crude product. The crude product was further purified by silica gel column chromatography using a mixed medium of petroleum ether and EtOAc to give the desired products (3–27).

General procedure for aldehyde–amine–acetylene (A³) coupling reaction for the synthesis of monoamine oxidase B inhibitor pargyline

In a typical catalysis run, calculated amount of metal–NHC pre-catalyst **1a/1b/2a/2b** (0.02 mmol, 1 mol %) was dissolved in 5 mL of toluene and to this solution TMS acetylene (2.00 mmol) was added and stirred for 15 minutes followed by addition of formaldehyde (2.00 mmol) and N-methylbenzylamine (2.00 mmol) in the respective order and was stirred at 100 °C for 16 h. After that it was cooled down to room temperature, the solvent was evaporated and redissolved in 5 mL of CH₃OH, followed by the addition of K₂CO₃ (10.0 mmol). The resulting reaction mixture was stirred at room temperature for 3 h. The reaction was quenched with Et₂O, extracted with 2 × 10 mL of CH₂Cl₂, the combined organic fraction was dried over Na₂SO₄, and the volatiles were removed under reduced pressure to obtain crude product. The crude product was further purified by silica gel column chromatography using a mixed medium of petroleum ether and EtOAc to give the desired product (**28**).

General procedure for aldehyde–amine-acetylene (A³) coupling reaction for the gram-scale synthesis of monoamine oxidase B inhibitor pargyline

In a typical catalysis run, calculated amount of metal–NHC pre-catalyst **1a** (0.1 mmol, 1 mol %) was dissolved in 5 mL of toluene and to this solution TMS acetylene (10.0 mmol) was added and stirred for 15 min followed by addition of formaldehyde (10.0 mmol) and N-methylbenzylamine (10.0 mmol) in the respective order and was stirred at 100 °C for 16 h. After that it was cooled down to room temperature, redissolved in 15 mL of CH₃OH and K₂CO₃ (50.0 mmol) was added to it. The resulting reaction mixture was stirred at room temperature for 3 h. The reaction was quenched with Et₂O, extracted with 2 × 50 mL of CH₂Cl₂, the combined organic fraction was dried over Na₂SO₄, and the volatiles were removed under reduced pressure to obtain crude product. The crude product was further purified by silica gel column chromatography using a mixed medium of petroleum ether and EtOAc to give the desired product (**28**) (1.01 g, 63 %).

4.1. Computational studies

In this study, Gaussian 09 Revision D.01 [66] was used for performing all DFT calculations, while Orca 5.0 version software [77,78] was chosen specifically for spectroscopic calculations, including ¹³C NMR analyses. Grimme's dispersion-corrected B3LYP functional (B3LYP-D3) was employed for geometry optimization [70,71]. (Supporting Information Tables S9-S14). Geometry optimization and computation of imaginary frequencies were conducted for all entities, encompassing copper (1–2)**a** and the silver (1–2)**b** complexes, intermediates, and transition states. The calculations were conducted using the SDD basis set for copper and silver metal [72] and the 6–31G* basis set for elements such as C, H, N, O, and Br [70,71,73,74]. Frequency calculations were executed to pinpoint minima on the potential-energy surface (PES) and to determine the Gibbs free energy correction. Furthermore, we incorporated solvation energy into the gas phase energy (Gibbs free energy correction) by employing a more advanced level of theory (B3LYP-D3/SDD, TZVP) [75]. Solvation energy was determined using the polarizable continuum model (PCM) in conjunction with the solvent toluene [76]. The PCM model accounts for solvation-free energy by evaluating electrostatic, dispersion-repulsion, and cavitation terms. The choice of toluene as the solvent aligns with the experimental conditions as reported. We employed two software applications, Chemcraft 1.6 [92] and Gaussview 6.0 [93], to visualize the optimized geometries effectively. Furthermore, Gaussian 09 software was utilized to conduct thorough NBO (Natural Bond Orbital) [94] and WBI (Wiberg Bond Index) analyses [95] using DFT methods. The NBO analysis offered detailed insights into the characteristics of bonding orbitals and provided valuable information about the distribution of natural charges within the system. On the other hand, WBI analysis provided bond index values that elucidated the nature of the bonds, indicating whether they are single, double, or triple bonds. The optimized geometry coordinates has been given in the Supporting Information Tables S9-S14.

The non-covalent interactions (NCI) analysis has been done by Multiwfn 3.8 [96] and VMD software [97]. The default reduced density gradient (RDG) isosurface value 0.5, and the color range (–0.035 to 0.02) were taken in calculation. The steric map plot calculations were performed using the SambVca 2.0 tool [88], specifically designed for analysing catalytic pockets through topographic steric maps. The XYZ coordinates required for generating steric map plots were derived from optimized geometries obtained through Gaussian 09 [66]. The SambVca 2.0 web tool establishes a correlation between steric effects and the percentage of buried volume (% V_{Bur}). Colour transitions from red to blue on the steric map plot indicate a decrease in steric influence, while the reverse trend is denoted by blue to red shifts. Flexibility in the steric map plot's customization is facilitated by adjusting parameters like atomic radii, sphere radius, and mesh spacing for numerical integration according to specific needs. In our study, we adhered to the default settings, and it's important to note that our calculations encompassed hydrogen atoms in the input, ensuring a comprehensive analysis.

For the purpose of conducting ¹³C NMR calculations using ORCA 5.0 software [77,78], we opted for the hybrid Generalized Gradient Approximation (GGA) B3LYP functional [70,71,74]. Within our study, we employed the Resolution of Identity (RI) approximation, specifically utilizing the RIJCOSX approximation [98]. Our choice of basis sets for the ¹³C NMR calculations included SARC-ZORA-TZVPP for silver and copper metals [79,80], ZORA-def2-TZVP for chlorine and bromine atoms [81], IGLO-II for carbon atoms [82,83], and ZORA-def2-SVP for silicon, oxygen, nitrogen, and hydrogen atoms [84]. An essential detail to highlight is that the optimized coordinates obtained from Gaussian 09 software [66] were utilized as the foundation for our ¹³C NMR calculations. This decision ensured both consistency and precision in our analytical outcomes.

Supporting Information

General procedure for blank run, control runs, mercury-drop experiment, mass experiment for the detection of catalytic intermediates and XPS experiments, and analytical data of catalysis products (**3–28**), ¹H NMR, ¹³C{¹H} NMR, IR, HRMS, elemental analysis data of the compounds (1–2)**a**, and (1–2)**b**, and ¹H NMR, Mass data, and elemental analysis data of the catalysis products (**3–28**); X-ray crystallographic data for the complexes CCDC-2218967 (for **1b**), CCDC-2218671 (for **2a**), CCDC-2218670 (for **2b**), (CIF), Steric map plot for copper (1–2)**a** and the silver (1–2)**b** complexes, ¹³C NMR calculations for copper (1–2)**a** and the silver (1–2)**b** complexes, ChemDraw mechanism for A³ coupling reaction of cyclic/acyclic secondary amines, aliphatic/aromatic aldehydes, and phenylacetylene substrates, the DFT method optimized coordinates, natural charges, NBO plots, WBI value, NCI calculations, and structural parameters of species copper (1–2)**a** and the silver (1–2)**b**, reactant complex (RC), transition states (TS1), (TS2) and intermediates (Int1), (Int2), and the energy profile diagrams for the A³ coupling proposed pathway, can be found with this article. The X-ray crystallographic data can be obtained free of charge from the Cambridge Crystallographic Data centre via www.ccdc.cam.ac.uk/data_request/cif.

CRediT authorship contribution statement

Rajesh Manne: Investigation. **Sunita Sharma:** Investigation. **Shreyata Dey:** Investigation. **Sagar K. Patil:** Investigation. **Nidhi Nehra:** Investigation. **Hemant Rawool:** Investigation. **Gopalan Rajaraman:** Project administration. **Prasenjit Ghosh:** Project administration.

Declaration of competing interest

The authors declare that they have no known competing financial interests or personal relationships that could have appeared to influence the work reported in this paper.

Data availability

No data was used for the research described in the article.

Acknowledgements

We thank the Department of Science and Technology and Science and Engineering Research Board (Grant No: SR/ S1/IC-50/2011, EMR/2014/000254, CRG/2019/000029, CRG/2023/000012 and SB/SJF/2019-20/12) New Delhi, India and Council of Scientific & Industrial Research (CSIR) {01(2880)/ 17/EMR-II, and 01/3098/23/EMR II} New Delhi, India for financial support of this research. We acknowledge the Single Crystal X-ray Diffraction Facility, Department of Chemistry, IIT Bombay, Mumbai, India, for the crystallographic characterization data. We acknowledge the Central Surface Analytical Facility of IIT Bombay, Mumbai, India, for the X-ray Photoelectron Spectroscopy characterization data. We gratefully acknowledge the HPC Facility, IIT Bombay, Mumbai, India, for the computational calculation data. SS and HR thank the UGC, New Delhi, India, for the research fellowship. SD thanks IIT Bombay for the doctoral research fellowship. RM thanks SERB for the fellowship. SP and NN thank IIT Bombay, Mumbai, India, for the Institute Postdoctoral Fellowship.

Supplementary materials

Supplementary material associated with this article can be found, in the online version, at [doi:10.1016/j.molstruc.2024.139022](https://doi.org/10.1016/j.molstruc.2024.139022).

References

- T. Tábi, L. Vécsei, M.B. Youdim, P. Riederer, É. Szökő, Selegiline: a molecule with innovative potential, *J. Neural Transm.* 127 (5) (2020) 831–842.
- S. Xie, J. Chen, X. Li, T. Su, Y. Wang, Z. Wang, L. Huang, X. Li, Synthesis and evaluation of selegiline derivatives as monoamine oxidase inhibitor, antioxidant and metal chelator against Alzheimer's disease, *Bioorg. Med. Chem.* 23 (13) (2015) 3722–3729.
- N.B. Kondekar, P. Kumar, Synthesis of (R)-selegiline via hydrolytic kinetic resolution, *Synth. Commun.* 41 (9) (2011) 1301–1308.
- L.M. Chahine, M.B. Stern, Rasagiline in Parkinson's disease, in: M.B.H. Youdim, P. Douce (Eds.), *International Review of Neurobiology*, Academic Press 2011, pp. 151–168.
- I. Denya, S.F. Malan, A.B. Enogieru, S.I. Omoruyi, O.E. Ekpo, E. Kapp, F.T. Zindo, J. Joubert, Design, synthesis and evaluation of indole derivatives as multifunctional agents against Alzheimer's disease, *Medchemcomm.* 9 (2) (2018) 357–370.
- O. Weinreb, T. Amit, O. Bar-Am, M.B.H. Youdim, A novel anti-Alzheimer's disease drug, ladostigil: neuroprotective, multimodal brain-selective monoamine oxidase and cholinesterase inhibitor, in: M.B.H. Youdim, P. Douce (Eds.), *A novel anti-Alzheimer's disease drug, ladostigil: neuroprotective, multimodal brain-selective monoamine oxidase and cholinesterase inhibitor*, *Int. Rev. Neurobiol.* (2011) 191–215.
- M. Weinstock, L. Luques, C. Bejar, S. Shoham, Ladostigil, a Novel Multifunctional Drug For the Treatment of Dementia Co-Morbid With Depression, in: P. Riederer, H. Reichmann, M.B.H. Youdim, M. Gerlach (Eds.), *Parkinson's Disease and Related Disorders*, Springer Vienna, Vienna, 2006, pp. 443–446.
- M. Naoi, W. Maruyama, M. Shamoto-Nagai, Neuroprotective function of rasagiline and selegiline, inhibitors of Type B monoamine oxidase, and role of monoamine oxidases in synucleinopathies, *Int. J. Mol. Sci.* (2022).
- G. Ma, Z. Xu, P. Zhang, J. Liu, X. Hao, J. Ouyang, P. Liang, S. You, X. Jia, A novel synthesis of rasagiline via a chemoenzymatic dynamic kinetic resolution, *Org. Process. Res. Dev.* 18 (10) (2014) 1169–1174.
- Y. Volkova, S. Baranin, I. Zavarzin, A3 coupling reaction in the synthesis of heterocyclic compounds, *Adv. Synth. Catal.* 363 (1) (2021) 40–61.
- J. Farhi, I.N. Lykakis, G.E. Kostakis, Metal-catalysed A3 coupling methodologies: classification and visualisation, *Catalysts*, 2022.
- B.V. Rokade, J. Barker, P.J. Guiry, Development of and recent advances in asymmetric A3 coupling, *Chem. Soc. Rev.* 48 (18) (2019) 4766–4790.
- J.-N. Mo, J. Su, J. Zhao, The asymmetric A3(Aldehyde-Alkyne-Amine) coupling: highly enantioselective access to propargylamines, *Molecules* (2019).
- A. Mariconda, M. Sirignano, C. Costabile, P. Longo, New NHC- silver and gold complexes active in A3-coupling (aldehyde-alkyne-amine) reaction, *Mol. Catal.* 480 (2020) 110570.
- V.A. Peshkov, O.P. Pereshivko, E.V. Van der Eycken, A walk around the A3-coupling, *Chem. Soc. Rev.* 41 (10) (2012) 3790–3807.
- M.M. Rahman, G. Meng, E. Bisz, B. Dziuk, R. Lalancette, R. Szostak, M. Szostak, ItOct (ItOctyl) – pushing the limits of ItBu: highly hindered electron-rich N-aliphatic N-heterocyclic carbenes, *Chem. Sci.* 14 (19) (2023) 5141–5147.
- Q. Zhao, G. Meng, G. Li, C. Flach, R. Mendelsohn, R. Lalancette, R. Szostak, M. Szostak, IPr# – highly hindered, broadly applicable N-heterocyclic carbenes, *Chem. Sci.* 12 (31) (2021) 10583–10589.
- S. Dierick, D.F. Dewez, I.E. Markó, IPr*(2-Np)—An exceedingly bulky n-heterocyclic carbene, *Organometallics* 33 (3) (2014) 677–683.
- G. Berthon-Gelloz, M.A. Siegler, A.L. Spek, B. Tinant, J.N.H. Reek, I.E. Markó, IPr* an easily accessible highly hindered N-heterocyclic carbene, *Dalton Trans.* 39 (6) (2010) 1444–1446.
- A. Beillard, F. Quintin, J. Gatignol, P. Retailleau, J.-L. Renaud, S. Gaillard, T.-X. Métro, F. Lamaty, X. Bantrel, Solving the challenging synthesis of highly cytotoxic silver complexes bearing sterically hindered NHC ligands with mechanochemistry, *Dalton Trans.* 49 (36) (2020) 12592–12598.
- G. Wang, L. Pecher, G. Frenking, H.V.R. Dias, Vinyltrifluoroborate complexes of silver supported by N-heterocyclic carbenes, *Eur. J. Inorg. Chem.* 2018 (37) (2018) 4142–4152.
- D. Guest, M.-T. Chen, G.J. Tizzard, S.J. Coles, M.L. Turner, O. Navarro, [(1,3-Bis(2,6-bis(diphenylmethyl)-4-methylphenyl)imidazole-2-ylidene)PdCl2(NEt3)]: “Throwing Away” a different ancillary ligand to enhance the catalytic activity at room temperature, *Eur. J. Inorg. Chem.* 2014 (13) (2014) 2200–2203.
- T.G. Carroll, D.E. Ryan, J.D. Erickson, R.M. Bullock, B.L. Tran, Isolation of a Cu–H monomer enabled by remote steric substitution of a N-heterocyclic carbene ligand: stoichiometric insertion and catalytic hydroboration of internal alkenes, *J. Am. Chem. Soc.* 144 (30) (2022) 13865–13873.
- M. Dolna, M. Nowacki, O. Danylyuk, A. Brotons-Rufes, A. Poater, M. Michalak, NHC–BIAN–Cu(I)-catalyzed friedländer-type annulation of 2-amino-3-(per)fluoroacetylpyridines with alkynes on water, *J. Org. Chem.* 87 (9) (2022) 6115–6136.
- A. Gómez-Suárez, R.S. Ramón, O. Songis, A.M.Z. Slawin, C.S.J. Cazin, S.P. Nolan, Influence of a very bulky N-heterocyclic carbene in gold-mediated catalysis, *Organometallics* 30 (20) (2011) 5463–5470.
- A. Collado, S.R. Patrick, D. Gasperini, S. Meiries, S.P. Nolan, Influence of bulky yet flexible N-heterocyclic carbene ligands in gold catalysis, *Beilstein. J. Org. Chem.* 11 (2015) 1809–1814.
- S. Ray, R. Mohan, J.K. Singh, M.K. Samantary, M.M. Shaikh, D. Panda, P. Ghosh, Anticancer and antimicrobial metallopharmaceutical agents based on palladium, gold, and silver N-heterocyclic carbene complexes, *J. Am. Chem. Soc.* 129 (48) (2007) 15042–15053.
- A. Kumar, A. Naaz, A.P. Prakasham, M.K. Gangwar, R.J. Butcher, D. Panda, P. Ghosh, Potent anticancer activity with high selectivity of a chiral palladium N-heterocyclic carbene complex, *ACS Omega* 2 (8) (2017) 4632–4646.
- A. John, P. Ghosh, Fascinating frontiers of N/O-functionalized N-heterocyclic carbene chemistry: from chemical catalysis to biomedical applications, *Dalton Trans.* 39 (31) (2010) 7183–7206.
- A. Kumar, P. Ghosh, Studies of the electronic properties of N-heterocyclic carbene ligands in the context of homogeneous catalysis and bioorganometallic chemistry, *Eur. J. Inorg. Chem.* 2012 (25) (2012) 3955–3969.
- B. Ramasamy, P. Ghosh, The developing concept of bifunctional catalysis with transition metal N-heterocyclic carbene complexes, *Eur. J. Inorg. Chem.* 2016 (10) (2016) 1448–1465.
- M.N. Rao, R. Manne, J.M. Tanski, R. Butcher, P. Ghosh, One pot synthesis of propargylamines by three component amine-aldehyde-acetylene (A3) coupling catalyzed by neutral Ag(I) and Au(I) and cationic Pd(II) and Ni(II) complexes of a pincer N-heterocyclic carbene, *Mol. Catal.* 529 (2022) 112515.
- A. Kumar, M.K. Gangwar, A.P. Prakasham, D. Mhatre, A.C. Kalita, P. Ghosh, Accessing a biologically relevant benzofuran skeleton by a one-pot tandem heck alkynylation/cyclization reaction using well-defined palladium N-heterocyclic carbene complexes, *Inorg. Chem.* 55 (6) (2016) 2882–2893.
- C. Singh, A.P. Prakasham, M.K. Gangwar, R.J. Butcher, P. Ghosh, One-pot tandem hiyama alkynylation/cyclizations by palladium(II) acyclic diaminocarbene (ADC) complexes yielding biologically relevant benzofuran scaffolds, *ACS Omega* 3 (2) (2018) 1740–1756.
- C. Singh, A.P. Prakasham, P. Ghosh, Palladium acyclic diaminocarbene (ADC) triflate complexes as effective precatalysts for the hiyama alkynylation/cyclization reaction yielding benzofuran compounds: probing the influence of the triflate coligand in the one-pot tandem reaction, *ChemistrySelect.* 4 (1) (2019) 329–336.
- A.P. Prakasham, S. Ta, S. Dey, P. Ghosh, One pot tandem dual C/C and C/O bond reductions in the β -alkylation of secondary alcohols with primary alcohols by ruthenium complexes of amido and picolyl functionalized N-heterocyclic carbenes, *Dalton Trans.* 50 (43) (2021) 15640–15654.
- A. Kumar, S. Ta, C. Nettem, J.M. Tanski, G. Rajaraman, P. Ghosh, One pot tandem dehydrogenative cross-coupling of primary and secondary alcohols by ruthenium amido-functionalized 1,2,4-triazole derived N-heterocyclic carbene complexes, *RSC Adv.* 12 (45) (2022) 28961–28984.
- S. Dey, P. Ghosh, Accessing heteroannular benzoxazole and benzimidazole scaffolds via carbodiimides using azide–isocyanide cross-coupling as catalyzed by mesoionic singlet palladium carbene complexes derived from a phenothiazine moiety, *ACS Omega* 8 (12) (2023) 11039–11064.
- J. Singh, S. Sharma, A.P. Prakasham, G. Rajaraman, P. Ghosh, Accessing bioactive hydrazones by the hydrohydrazination of terminal alkynes catalyzed by gold(I) acyclic aminoxy carbene complexes and their gold(I) arylthiolato and gold(III) tribromo derivatives: a combined experimental and computational study, *ACS Omega* 8 (23) (2023) 21042–21073.

- [40] C. Yuan, X. Zhao, G. Nan, Silver-catalyzed multicomponent reactions for the construction of γ -carbonyl- α -amino acid derivatives, *Tetrahedron. Lett.* 61 (39) (2020) 152318.
- [41] C. Wei, J.T. Mague, C.-J. Li, Cu (I) -catalyzed direct addition and asymmetric addition of terminal alkynes to imines, *Proc. Natl. Acad. Sci.* 101(16) (2004) 5749–5754.
- [42] A. Rühling, H.J. Galla, F. Glorius, A remarkably simple hybrid surfactant–NHC ligand, its gold-complex, and application in micellar catalysis, *Chem.–A Eur. J.* 21 (35) (2015) 12291–12294.
- [43] N. Parvin, N. Sen, S. Tothadi, S. Muhammed, P. Parameswaran, S. Khan, Synthesis and application of silylene-stabilized low-coordinate Ag(I)–arene cationic complexes, *Organometallics* 40 (11) (2021) 1626–1632.
- [44] A. Mariconda, M. Sirignano, C. Costabile, P. Longo, Effect of counterion on the catalytic activity of Nhc-Gold (I) in A3 coupling reactions, Available at SSRN 4502669.
- [45] C. Costabile, A. Mariconda, M. Sirignano, A. Crispini, F. Scarpelli, P. Longo, A green approach for A3-coupling reactions: an experimental and theoretical study on NHC silver and gold catalysts, *N. J. Chem.* 45 (39) (2021) 18509–18517.
- [46] C. Zhang, S. Yu, F. Wang, J. Cao, X. Liang, F. Wang, H. Zheng, Y. Zhang, M. Yang, B. Zhao, Insights into the three-component coupling reactions of aldehydes, alkynes, and amines catalyzed by N-heterocyclic carbene silver: a DFT study, *Catalysts* 13 (4) (2023) 646.
- [47] M.E. Agbo, H.N. Heinz, J.B. Mather, J. Fotie, Tandem Cu–Zinc dust as a sustainable catalyst for the preparation of propargylamine derivatives via an A3 coupling reaction, under neat conditions, *Tetrahedron Green Chem.* (2023) 100027.
- [48] B. Cordero, V. Gomez, A.E. Platero-Prats, M. Reves, J. Echeverria, E. Cremades, F. Barragan, S. Alvarez, Covalent Radii Revisited, *Dalton Trans.* (21) (2008) 2832–2838.
- [49] U.M. Tripathi, A. Bauer, H. Schmidbaur, Covalent radii of four-co-ordinate copper (I), silver(I) and gold(I): crystal structures of [Ag(AsPh₃)₄]BF₄ and [Au(AsPh₃)₄]BF₄, *J. Chem. Soc.* 17 (1997) 2865–2868. *Dalton Transactions.*
- [50] M. Mateus, A. Kiss, I. Čisárová, T.M. Karpiński, L. Rycek, Synthesis of silver complexes with chelating bidentate N-heterocyclic ligands, their application in catalytic A3 coupling, and as antimicrobial agents, *Appl. Organomet. Chem.* 37 (4) (2023) e6994.
- [51] M. Sirignano, A. Mariconda, G. Vigliotta, J. Ceramella, D. Iacopetta, M.S. Sinicropi, P. Longo, Catalytic and biological activity of silver and gold complexes stabilized by NHC with hydroxy derivatives on nitrogen atoms, *Catalysts* (2022).
- [52] Y. Li, X. Chen, Y. Song, L. Fang, G. Zou, Well-defined N-heterocyclic carbene silver halides of 1-cyclohexyl-3-arylmethylimidazolylidene: synthesis, structure and catalysis in A3-reaction of aldehydes, amines and alkynes, *Dalton Trans.* 40 (9) (2011) 2046–2052.
- [53] R. Kılıncarslan, N. Sadiç, Catalytic activity of N-heterocyclic carbene silver complexes derived from imidazole ligands, *Inorg. Nano-Metal Chem.* 47 (3) (2017) 462–466.
- [54] G.A. Price, A.K. Brisdon, S. Randall, E. Lewis, D.M. Whittaker, R.G. Pritchard, C. A. Muryn, K.R. Flower, P. Quayle, Some insights into the gold-catalysed A3-coupling reaction, *J. Organomet. Chem.* 846 (2017) 251–262.
- [55] M.-T. Chen, B. Landers, O. Navarro, Well-defined (N-heterocyclic carbene)–Ag(I) complexes as catalysts for A3 reactions, *Org. Biomol. Chem.* 10 (11) (2012) 2206–2208.
- [56] M.-T. Chen, O. Navarro, N-Heterocyclic Carbene, (NHC)–Copper(I) complexes as catalysts for A3 reactions, *Synlett* 24 (10) (2013) 1190–1192.
- [57] F. Lazreg, F. Nahra, C.S.J. Cazin, Copper–NHC complexes in catalysis, *Coord. Chem. Rev.* 293–294 (2015) 48–79.
- [58] P. Li, L. Wang, Y. Zhang, M. Wang, Highly efficient three-component (aldehyde–alkyne–amine) coupling reactions catalyzed by a reusable PS-supported NHC–Ag(I) under solvent-free reaction conditions, *Tetrahedron. Lett.* 49 (47) (2008) 6650–6654.
- [59] T.J. Williams, J.T.W. Bray, B.R.M. Lake, C.E. Willans, N.A. Rajabi, A. Ariafard, C. Manzini, F. Bellina, A.C. Whitwood, L.J.S. Fairlamb, Mechanistic elucidation of the arylation of non-spectator N-heterocyclic carbenes at copper using a combined experimental and computational approach, *Organometallics* 34 (14) (2015) 3497–3507.
- [60] C.A. Citadelle, E.L. Nouy, F. Bisaro, A.M.Z. Slawin, C.S.J. Cazin, Simple and versatile synthesis of copper and silver N-heterocyclic carbene complexes in water or organic solvents, *Dalton Trans.* 39 (19) (2010) 4489–4491.
- [61] J. Liu, R. Zhang, S. Wang, W. Sun, C. Xia, A general and efficient copper catalyst for the double carbonylation reaction, *Org. Lett.* 11 (6) (2009) 1321–1324.
- [62] D.V. Partyka, N. Deligoul, Phosphine- and carbene-ligated silver acetate: easily-accessed synthons for reactions with silylated nucleophiles, *Inorg. Chem.* 48 (19) (2009) 9463–9475.
- [63] R.R. Narra, V.G. Unnithan, T.H. Wong, Z. Guo, Thiamine carbene liganded gold(I) chloride catalyzes an efficient aldehyde–alkyne–amine coupling reaction in water, *Green Chem.* 25 (5) (2023) 1920–1924.
- [64] X.Q. Chen, Z. Li, S.X. Dou, Ambient facile synthesis of gram-scale copper selenide nanostructures from commercial copper and selenium powder, *ACS Appl. Mater. Interfaces* 7 (24) (2015) 13295–13302.
- [65] J. Cao, G. Xu, P. Li, M. Tao, W. Zhang, Polyacrylonitrile fiber supported N-heterocyclic carbene Ag(I) as efficient catalysts for three-component coupling and intramolecular 1,3-dipolar cycloaddition reactions under flow conditions, *ACS Sustain. Chem. Eng.* 5 (4) (2017) 3438–3447.
- [66] M.J. Frisch, G.W. Trucks, H.B. Schlegel, G.E. Scuseria, M.A. Robb, J.R. Cheeseman, G. Scalmani, V. Barone, B. Mennucci, G. Petersson, Gaussian 09, Revision D. 01, Gaussian, Inc., Wallingford CT, See also: URL: <http://www.gaussian.com> (2009).
- [67] M.J.T. Frisch, G.W. Schlegel, H.B. Scuseria, G.E. Robb, M.A. Cheeseman, J.R. Scalmani, G. Barone, V. Mennucci, B. Petersson, G.A. Nakatsuji, H. Caricato, M. Li, X. Hratchian, H.P. Izmaylov, A.F. Bloino, J. Zheng, G. Sonnenberg, J.L. Hada, M. Ehara, M. Toyota, K. Fukuda, R. Hasegawa, J. Ishida, M. Nakajima, T. Honda, Y. Kitao, O. Nakai, H. Vreven, T. Montgomery, J.A. Peralta, J.E. Ogliaro, F. Bearpark, M. Heyd, J.J. Brothers, E. Kudin, K.N. Staroverov, V.N. Kobayashi, R. Normand, J. Raghavachari, K. Rendell, A. Burant, J.C. Iyengar, S.S. Tomasi, J. Cossi, M. Rega, N. Millam, J.M. Klene, M. Knox, J.E. Cross, J.B. Bakken, V.; Adamo, C.; Jaramillo, J.; Gomperts, R.; Stratmann, R. E.; Yazyev, O.; Austin, A. J.; Cammi, R.; Pomelli, C.; Ochterski, J. W.; Martin, R. L.; Morokuma, K.; Zakrzewski, V. G.; Voth, G. A.; Salvador, P.; Dannenberg, J. J.; Dapprich, S.; Daniels, A. D.; Farkas, O.; Foresman, J. B.; Ortiz, J. V.; Cioslowski, J.; Fox, D. J., Gaussian 09, Revision A.1, Gaussian, Inc., Wallingford CT, 2009.
- [68] M. Caricato, M.J. Frisch, J. Hiscokcs, M.J. Frisch, Gaussian 09: IOps Reference, Gaussian Wallingford, CT, USA2009.
- [69] G. Zheng, L. Sonnenberg, M. Hada, M. Ehara, K. Toyota, Gaussian 09, R. Fukuda, J. Hasegawa, M. Ishida, T. Nakajima, Y. Honda, Gaussian Inc., Wallingford CT, 2009, p. 48.
- [70] A.D. Becke, Density-functional thermochemistry. V. Systematic optimization of exchange-correlation functionals, *J. Chem. Phys.* 107 (20) (1997) 8554–8560.
- [71] J. Antony, S. Grimme, Density functional theory including dispersion corrections for intermolecular interactions in a large benchmark set of biologically relevant molecules, *Phys. Chem. Chem. Phys.* 8 (45) (2006) 5287–5293.
- [72] L.E. Roy, P.J. Hay, R.L. Martin, Revised basis sets for the LANL effective core potentials, *J. Chem. Theory. Comput.* 4 (7) (2008) 1029–1031.
- [73] A.V. Mitin, J. Baker, P. Pulay, An improved 6-31 G* basis set for first-row transition metals, *J. Chem. Phys.* 118 (17) (2003) 7775–7782.
- [74] A.D. Becke, Density-functional exchange-energy approximation with correct asymptotic behavior, *Phys. Rev. A* 38 (6) (1988) 3098–3100.
- [75] M.R. Silva-Junior, M. Schreiber, S. Sauer, W. Thiel, Benchmarks of electronically excited states: basis set effects on CASPT2 results, *J. Chem. Phys.* 133 (17) (2010).
- [76] J. Tomasi, B. Mennucci, R. Cammi, Quantum mechanical continuum solvation models, *Chem. Rev.* 105 (8) (2005) 2999–3094.
- [77] F. Neese, F. Wennmohs, U. Becker, C. Riplinger, The ORCA quantum chemistry program package, *J. Chem. Phys.* 152 (22) (2020) 224108.
- [78] F. Neese, Software update: the ORCA program system—Version 5.0, *Wiley Interdisc. Rev.: Comput. Mol. Sci.* 12 (5) (2022) e1606.
- [79] J.D. Roloff, F. Neese, D.A. Pantazis, All-electron scalar relativistic basis sets for the elements Rb–Xe, *J. Comput. Chem.* 41 (20) (2020) 1842–1849.
- [80] S.D. Waniek, C. Förster, K. Heinze, Protic ferrocenyl acyclic diamino carbene Gold (I) complexes, *Eur. J. Inorg. Chem.* 2022 (2) (2022) e202100905.
- [81] M.Z. Sadvakassova, A.I. Khlebnikov, A.A. Bakibaev, O.A. Kotelnikov, R.S. Erkasov, M.A. Yelubay, M.A. Issabayeva, Rotational barriers in N-benzhydroylformamides: an NMR and DFT study, *Molecules* 28 (2) (2023) 535.
- [82] L.B. Krivdin, Computational protocols for calculating ¹³C NMR chemical shifts, *Prog. Nucl. Magn. Reson. Spectrosc.* 112 (2019) 103–156.
- [83] M. Kaupp, O.L. Malkin, V.G. Malkin, On the importance of spin-orbit coupling and electron correlation, *Chem. Phys. Lett.* 265 (1–2) (1997) 55–59.
- [84] J.A. Laub, K.D. Vogiatzis, Theoretical investigation of actinide ligation in aqueous and organic phase for nuclear waste treatment, *J. Phys. Chem. A* 127 (26) (2023) 5523–5533.
- [85] M. Beytur, I. Avinca, Molecular, Electronic, Nonlinear Optical and Spectroscopic Analysis of Heterocyclic 3-Substituted-4-(3-methyl-2-thienylmethyleneamino)-4,5-dihydro-1H-1,2,4-triazol-5-ones: Experiment and DFT Calculations, *27(1)* (2021) 1–16.
- [86] B.-B. Gu, W. Wu, F.-R. Jiao, W.-h. Jiao, L. Li, F. Sun, S.-P. Wang, F. Yang, H.-W. Lin, Aspergillone, an 8(14–15)-abeo-ergostane from the sponge-derived fungus *Aspergillus flocculosus* 16D-1, *J. Org. Chem.* 84 (1) (2019) 300–306.
- [87] S.A. Kondrashova, F.M. Polyancev, Y.S. Ganushevich, S.K. Latypov, DFT approach for predicting ¹³C NMR shifts of atoms directly coordinated to nickel, *Organometallics* 40 (11) (2021) 1614–1625.
- [88] L. Falivene, R. Credendino, A. Poater, A. Petta, L. Serra, R. Oliva, V. Scarano, L. Cavallo, SambVca 2. A web tool for analyzing catalytic pockets with topographic steric maps, *Organometallics* 35 (13) (2016) 2286–2293.
- [89] L. Falivene, Z. Cao, A. Petta, L. Serra, A. Poater, R. Oliva, V. Scarano, L. Cavallo, Towards the online computer-aided design of catalytic pockets, *Nat. Chem.* 11 (10) (2019) 872–879.
- [90] S. Dey, C.S. Nettem, G. Rajaraman, P. Ghosh, Convenient access to amidines by mesoionic singlet palladium carbene catalyzed hydrazone-isocyanide-amine (HIA) coupling: scope and mechanistic insights, *Mol. Catal.* 553 (2024) 113735.
- [91] G.M. Sheldrick, A short history of SHELX, *Acta Crystallogr., Sect. A: Found. Crystallogr.* 64 (1) (2008) 112–122.
- [92] G.A. Zhurko, D.A. Zhurko, Version 1.7 (Build 132), HTML, Chemcraft., 2014. www.chemcraftprog.com.
- [93] R. Dennington, T. Keith, J. Millam, GaussView, Semichem Inc, Shawnee Mission, KS, 2009.
- [94] E.D. Glendening, C.R. Landis, F. Weinhold, NBO 6.0: Natural bond orbital analysis program, *J. Comput. Chem.* 34 (16) (2013) 1429–1437.
- [95] I. Mayer, Bond orders and valences in the SCF theory: a comment, *Theor. Chim. Acta* 67 (4) (1985) 315–322.
- [96] T. Lu, F. Chen, Multiwfn: A multifunctional wavefunction analyzer, *J. Comput. Chem.* 33 (5) (2012) 580–592.
- [97] W. Humphrey, A. Dalke, K. Schulten, VMD: visual molecular dynamics, *J. Mol. Graph.* 14 (1) (1996) 33–38.
- [98] F. Neese, The ORCA program system, *Wiley Interdisc. Rev.: Comput. Mol. Sci.* 2 (1) (2012) 73–78.